**Title: 2'3'-cGAMP is an immunotransmitter produced by cancer cells and regulated by ENPP1**

**Authors:** Jacqueline A. Carozza[1,2]†, Volker Böhnert[2,3]†, Kelsey E. Shaw[2,3], Khanh C. Nguyen[4], Gemini Skariah[2,3], Jenifer A. Brown[2,5], Marjan Rafat[6], Rie von Eyben[6], Edward E. Graves[6], Jeffrey S. Glenn[4], Mark Smith[2] and Lingyin Li[2,3]*

**Affiliations:**

[1]Department of Chemistry, [2]Stanford ChEM-H, [3]Department of Biochemistry, [4]Departments of Medicine and Microbiology & Immunology, [5]Biophysics program, [6]Department of Radiation Oncology, Stanford University, School of Medicine, CA 94306 USA.

†These authors contributed equally to this work.

*To whom correspondence should be addressed. E-mail: lingyinl@stanford.edu

Abstract

2'3'-cyclic GMP-AMP (cGAMP) is characterized as an intracellular second messenger that is synthesized in response to cytosolic dsDNA and activates the innate immune STING pathway. Our previous discovery of its extracellular hydrolase ENPP1 hinted at the existence of extracellular cGAMP. Here, using mass spectrometry, we detected that cGAMP is continuously exported as a soluble factor by an engineered cell line but then efficiently cleared by ENPP1, explaining why it has escaped detection until now. By

developing a potent, specific, and cell impermeable ENPP1 inhibitor, we detected cGAMP export in cancer cell lines commonly used for mouse tumor models. In tumors, depletion of extracellular cGAMP using neutralizing proteins decreased tumor-associated dendritic cells. Boosting extracellular cGAMP by genetic knockout and pharmacological inhibition of ENPP1 increased tumor-associated dendritic cells, shrunk tumors, and synergized with ionizing radiation and anti-CTLA-4 to cure tumors. In conclusion, cGAMP is an anti-cancer immunotransmitter released by tumors and detected by host innate immunity.

## Introduction

The second messenger 2'3'-cyclic GMP-AMP (cGAMP)[1] plays pivotal roles in anti-viral and anti-cancer innate immunity. It is synthesized by the enzyme cyclic-GMP-AMP synthase (cGAS)[2] in response to double-stranded DNA (dsDNA) in the cytosol, which is a danger signal for intracellular pathogens and damaged or cancerous cells[3–7]. cGAMP binds and activates its endoplasmic reticulum (ER) surface receptor Stimulator of Interferon Genes (STING)[8] to activate production of Type 1 interferons (IFNs). These potent cytokines trigger downstream innate and adaptive immune responses to clear the threat.

In addition to activating STING within its cell of origin, cGAMP can spread to bystander cells through gap junctions in epithelial cells[9]. This cell-cell communication mechanism alerts adjacent cells of the damaged cell and also, unfortunately, accounts for the

spreading of drug-induced liver toxicity[10,11] and brain metastases[12]. In addition, cytosolic cGAMP can be packaged into budding viral particles and transmitted during the next round of infection[13,14]. In both transmission modes, cGAMP is never exposed to the extracellular space.

We previously identified the enzyme responsible for the only detectable cGAMP hydrolase activity to be ectonucleotide pyrophosphatase phosphodiesterase 1 (ENPP1)[15]. This finding was puzzling because ENPP1 is annotated as an extracellular enzyme both as a membrane-bound form anchored by a single-pass transmembrane domain and as a cleaved soluble protein in the serum[15]. cGAMP, which has two negative charges and presumably cannot passively cross the cell membrane, can enter cells to activate STING[16,17], suggesting that there are transport channels for cGAMP. Because it can enter cells, cGAMP analogs are currently being tested in clinical trials to treat metastatic solid tumors via intratumoral injections. Knowing that extracellular cGAMP can be imported and has anti-cancer effects, and that the dominant cGAMP hydrolase is extracellular, we hypothesized that cGAMP is exported to the extracellular space to signal other cells and is regulated by extracellular degradation.

Here we report direct evidence for cGAMP export by cancers and the role of extracellular cGAMP in anti-cancer immune detection. Using genetic knockout and pharmacological inhibition, we also investigated the role of ENPP1 in controlling extracellular cGAMP concentration, immune infiltration, and tumor progression. Together, we characterize cGAMP as an immunotransmitter regulated by ENPP1.

## Results

### cGAMP is exported from 293T cGAS ENPP1$^{-/-}$ cells as a soluble factor

To test the hypothesis that cGAMP is present extracellularly, we first developed a liquid chromatography-tandem mass spectrometry (LC-MS/MS) method to detect cGAMP from complex mixtures. Using two isotopically labeled cGAMP standards (Fig. 1a), we can quantify cGAMP concentrations down to 0.5 nM in both basal cell culture media and serum containing media, and we can quantify intracellular cGAMP concentrations from cell extracts in the same experiment (Fig. 1b and Extended Data Fig. 1a, b)[18,19]. We chose to use 293T cells, which do not express cGAS or STING. By stably expressing mouse cGAS and knocking out ENPP1 using CRISPR, we created a 293T cGAS ENPP1$^{low}$ cell line (Extended Data Fig. 1c). We then isolated a single clone to create a 293T cGAS ENPP1$^{-/-}$ cell line. (Extended Data Fig. 1c). We also used serum-free media because serum contains a proteolytically cleaved soluble form of ENPP1. Using this ENPP1-free cell culture system, we detected constant low micromolar basal intracellular cGAMP concentrations in the 293T cGAS ENPP1$^{-/-}$ cells without any stimulation (Fig. 1c). This is not surprising since multiple reports show that there is abundant cytosolic dsDNA in cancer cells as a result of erroneous DNA segregation[20–22]. After replenishing the cells with fresh media, we measured a linear increase of extracellular cGAMP concentrations to 100 nM after 30 h (Fig. 1d). At 30 h, the number of cGAMP molecules outside the cells was equal to the number inside (Fig. 1e). We detected negligible

amount of cell death based on extracellular lactose dehydrogenate (LDH) activity, suggesting that cGAMP in the media is exported by live cells (Fig. 1e). We calculated the export rate ($v_{export}$) to be 220 molecules cell$^{-1}$ s$^{-1}$ (Fig. 1f). Finally, cGAMP in the media can pass through a 10 kDa filter without any retention, which should retain extracellular vesicles and proteins, suggesting that cGAMP is exported as a freely soluble molecule (Fig. 1g).

To further confirm that extracellular cGAMP secreted by 293T cells is predominantly in a soluble form, but not in extracellular vesicles, we used CD14$^{+}$ human peripheral blood mononuclear cells (PBMCs) as a reporter. These cells have previously been shown to take up soluble cGAMP, which leads to IFN-β production[17]. We observed that CD14$^{+}$ PBMCs respond to submicromolar concentrations of soluble cGAMP by upregulating *IFNB1* (Extended Data Fig. 2). Conditioned media from DNA-transfected cGAS-expressing 293T cGAS ENPP1$^{low}$ cells, but not DNA-transfected cGAS-null 293T cells, induced *IFNB1* expression in CD14$^{+}$ cells, suggesting that the activity is a result of extracellular cGAMP produced by 293T cells (Fig. 1h, i). Addition of purified soluble recombinant mouse ENPP1 (mENPP1) (Extended Data Fig. 1d) depleted detectable cGAMP in the conditioned media and also ablated this activity (Fig. 1 h, j). Because soluble ENPP1 (MW = ~100 kDa) cannot permeate membranes and, thus, can only access soluble extracellular cGAMP, we conclude that 293T cells secrete soluble cGAMP. Together, our data demonstrate that this artificial cancer cell line keeps its intracellular cGAMP at a steady state by exporting it into the extracellular media as a soluble factor.

ENPP1 regulates only extracellular cGAMP

Since we were able to observe extracellular cGAMP for the first time when we knocked out ENPP1 from 293T cells and cultured them in ENPP1-free media, we then investigated whether only extracellular cGAMP is regulated by ENPP1. Despite its extracellular annotation, it is possible that ENPP1 could flip orientation on the membrane, as reported for a related enzyme CD38[23], or it could be active when being synthesized in the ER lumen and cGAMP may cross the ER membrane (Fig. 2a). To investigate the localization of ENPP1 activity, we transfected 293T cGAS ENPP1$^{-/-}$ cells with human *ENPP1* expression plasmid and confirmed its activity in whole cell lysates (Fig. 2b). In intact cells, ENPP1 expression depletes extracellular cGAMP, but does not affect the intracellular cGAMP concentration (Fig. 2c). Therefore, extracellular, but not intracellular, cGAMP is regulated by ENPP1 in these cells.

Development of a cell impermeable ENPP1 inhibitor

To study the physiological relevance of extracellular cGAMP and why it needs to be regulated by a specific hydrolase, we sought to manipulate its concentration by pharmacologically inhibiting ENPP1. We first tested a nonspecific ENPP1 inhibitor QS1[24,25] (Extended Data Fig. 3a). Although QS1 can inhibit extracellular cGAMP degradation in cells overexpressing ENPP1, it also partially blocked cGAMP export in ENPP1 knockout cells (Extended Data Fig. 3b). QS1 treated cells have elevated

intracellular cGAMP, demonstrating again that export is a significant mechanism to maintain cGAMP homeostasis in cancer cells. The export blockage activity excludes QS1 as a tool to study extracellular cGAMP. our export studies. We therefore designed a phosphonate analog, STF-1084, to chelate $Zn^{2+}$ at the ENPP1 catalytic site and to minimize cell permeability and avoid intracellular off-targets (Fig. 3a). STF-1084 has a $K_{i,app}$ of 110 ± 10 nM (Fig. 3b), which is ~60-fold more potent than QS1 (Extended Data Fig. 3a).

We confirmed that STF-1084 is cell impermeable by performing three independent permeability assays: the parallel artificial membrane permeability assay (PAMPA) (Extended Data Fig. 4a); the intestinal cells Caco-2 permeability assay (Extended Data Fig. 4b); and the epithelial cells MDCK permeability assay (Extended Data Fig. 4c). Compared to control compounds with high cell permeability and low cell permeability, STF-1084 falls into the category of impermeable compounds in all three assays. In addition, it has low activity towards the closely related ectonucleotidases alkaline phosphatase ($K_{i,app}$ > 100 μM) and ENPP2 ($K_{i,app}$ = 5.5 μM) (Extended Data Fig. 4d). Although we do not expect STF-1084 to have intracellular off-targets due to its low cell permeability, we tested its binding against a panel of 468 kinases to further determine its specificity. Despite its structural similarity to AMP, STF-1084 binds to only two kinases at 1 μM (Extended Data Fig. 4e). STF-1084 also shows high stability ($t_{1/2}$ > 159 min) in both human and mouse liver microsomes. Together, we demonstrated that STF-1084 is a potent, cell impermeable, specific, and stable ENPP1 inhibitor.

Next, we measured the efficacy of STF-1084 in maintaining extracellular cGAMP concentrations of ENPP1 overexpressing 293T cGAS cells and obtained an $IC_{50}$ value of 340 ± 160 nM (Fig. 3c) with 10 μM being sufficient to completely block extracellular cGAMP degradation (Fig. 3d). Unlike QS1, STF-1084 had no effect on intracellular cGAMP, demonstrating that it does not affect cGAMP export (Fig. 3d). STF-1084 is, therefore, an excellent ENPP1 inhibitor tool compound to specifically increase extracellular cGAMP concentrations.

Finally, we tested the efficacy of STF-1084 in boosting extracellular cGAMP signal detectable to $CD14^+$ PBMCs. We first confirmed that STF-1084 is not toxic to PBMCs at the concentrations used (Extended Data Fig. 4f). Conditioned media from ENPP1 overexpressing 293T cGAS cells failed to induce *IFNB1* expression in $CD14^+$ cells (Fig. 3e, f). However, STF-1084 rescued extracellular cGAMP levels in the media and induction of *IFNB1* expression in $CD14^+$ cells (Fig. 3f). These results demonstrate that the enzymatic activity of ENPP1, not potential scaffolding effects as a transmembrane protein, dampens response to extracellular cGAMP by $CD14^+$ PBMCs. Together, our data suggest that extracellular cGAMP levels can be decreased by ENPP1 expression and increased by ENPP1 inhibition, which affects the activation of $CD14^+$ PBMCs in vitro.

Cancer cells express cGAS and continuously export cGAMP in culture

To ultimately determine if extracellular cGAMP can function as a danger signal secreted by cancer cells in vivo, we first sought to identify tumor models that export cGAMP. We tested one human (MDA-MB-231) and three mouse cancer cell lines (E0771, MC38, and 4T1-Luc, which is a 4T1 cell line expressing luciferase for in vivo imaging) in culture, all of which express cGAS (Fig. 4a). Intracellular cGAMP concentrations in these cells are difficult to detect. However, with extra concentration and purification steps, we were able to detect 5.8 x $10^{-10}$ nmol/cell (~150 nM) intracellular cGAMP in 4T1-Luc cells (Fig. 4b). Knocking down cGAS using shRNA leads to decreased cGAS protein levels and decreased intracellular cGAMP levels, demonstrating that cGAS expression controls the amount of cGAMP present in the 4T1-Luc cells (Extended Data Fig. 5a, b). Using STF-1084 to inhibit cell surface and soluble ENPP1 in the cell culture media, we detected continuous cGAMP export in all of these cell lines and extracellular cGAMP levels reached ~6 x $10^{-9}$ nmol/cell (~10 nM when diluted into the media) in 48 h (Fig. 4c, d and Extended Data Fig. 5c, d). Remarkably, this is about 10-fold the amount of cGAMP present inside cells, suggesting that cancer cells efficiently clear out their cGAMP by export. Ionizing radiation (IR) has been shown to increase cytosolic DNA and activate cGAS-dependent IFN-β production in tumor cells[26,27]. Indeed, IR treatment also increased extracellular cGAMP production in 4T1-Luc cells after 48 hours (Fig. 4e and Extended Data Fig. 5e). Together, our data demonstrate that these cancer cell lines constantly produce and efficiently export cGAMP, and can be stimulated with IR to produce more extracellular cGAMP.

Sequestration of extracellular cGAMP decreases tumor-associated dendritic cells dependent on tumor cGAS and host STING

In tumors, the extracellular space is estimated to be 0.3–0.8-fold the volume of the intracellular space[28]. In cell culture, however, the volume of the extracellular space is approximately 250–1000-fold the volume of the intracellular space[29]. Our cell culture system is, therefore, diluting the extracellular space by 300–3000-fold compared to in the tumor microenvironment. Given this dilution factor and our measurement of nanomolar extracellular cGAMP exported by cancer cells in vitro, we predict that extracellular cGAMP in the tumor microenvironment can reach the micromolar range, which may lead to innate immune recognition of tumor cells. Recognizing the limits of our in vitro cell experiments, we turned to in vivo experiments to investigate the role of extracellular cGAMP (Fig. 5a). First, we sought to determine the importance of tumor versus host cGAMP by knocking out cGAS in tumor cells (Extended Data Fig. 6a) and utilized cGAS$^{-/-}$ and STING$^{-/-}$ mice in the C57BL/6 background. We also developed a neutralizing agent as a tool to specifically sequester extracellular cGAMP (Fig. 5a). We took advantage of the soluble cytosolic domain of STING (Fig. 5b), which binds cGAMP with a $K_d$ of 73 ± 14 nM (Fig. 5c). We also generated an R237A[16] mutant STING as a non-binding STING control (Fig. 5b-d)**.** To test the neutralizing efficacy of these proteins in cell culture, we used CD14$^+$ PBMCs. Wild type (WT) STING (neutralizing STING) was able to neutralize extracellular cGAMP with the predicted 2:1 stoichiometry, while the non-binding STING had no effect even when at a 200-fold higher concentration (Fig. 5e).

We established E0771 orthotopic tumors in mice, followed by intratumoral injection of neutralizing STING to deplete extracellular cGAMP, and excision of the tumors to stain for tumor-associated leukocytes. In WT E0771 tumors, neutralizing STING significantly decreased the CD11c$^{+}$ dendritic cell population in the total CD45$^{+}$/MHC-II$^{+}$ tumor-associated antigen presenting cell (APCs) population, suggesting that extracellular cGAMP can be detected by the immune system (Fig. 5f, g and Extended Data Fig. 6b). Extracellular cGAMP depletion also diminished the CD11c$^{+}$ population when tumors are grown in cGAS$^{-/-}$ mice, suggesting that host cells do not contribute significantly to extracellular cGAMP production (Fig. 5g and Extended Data Fig. 6b). In contrast, extracellular cGAMP depletion did not affect the CD11c$^{+}$ population when cGAS$^{-/-}$ E0771 cells (multiple clones were pooled to achieve clean knockout but minimize clonal effects) or STING$^{-/-}$ mice were used. This demonstrates that tumor cells, but not host cells, are the dominant producers of extracellular cGAMP, which is then sensed by host STING (Fig. 5g and Extended Data Fig. 6b). We also tested the orthotopic 4T1-Luc tumor model in the BALB/c background. Although cGAS and STING knockout strains have not been established in this background, we knocked out cGAS in the 4T1-Luc tumors. Intratumoral injection of neutralizing STING into the WT 4T1-Luc tumors significantly decreased the tumor-associated CD11c$^{+}$ population in the CD45$^{+}$/MHC II$^{+}$ population (Fig. 5h and Extended Data Fig. 6c). In contrast, extracellular cGAMP depletion had no effect in cGAS$^{-/-}$ 4T1-Luc tumors (Fig. 5h and Extended Data Fig. 6c). We also depleted extracellular cGAMP by intratumoral injection of mENPP1 protein (Extended Data Fig. 1d) and again observed diminished CD11c$^{+}$ cells in the

CD45$^+$/MHC II$^+$ population (Fig. 5i and Extended Data Fig. 6d). Results from our E0771 and 4T1-Luc models together demonstrate that extracellular cGAMP produced by tumor cells activates innate immune responses in a manner dependent on host STING but independent of host cGAS. Together, our data demonstrate that extracellular cGAMP produced by cancer cells is a danger signal that elicits innate immune responses.

Increasing extracellular cGAMP by reducing ENPP1 activity increases dendritic cell infiltration and renders breast tumors more treatable

ENPP1 is highly expressed in some breast cancers and its level has been correlated with poor prognosis[30–32]. High ENPP1 expression may be a mechanism breast cancers utilize to deplete extracellular cGAMP and dampen immune detection. We measured ENPP1 activities in three triple negative breast cancer cells 4T1-Luc, E0771, and MDA-MB-231, with MDA-MB-231 and 4T1-Luc exhibiting high ENPP1 activities (Extended Data Fig. 7a). We, therefore, chose the triple negative, metastatic, and orthotopic 4T1-Luc mouse model to probe the effect of ENPP1 on tumor immune detection, growth, and responses to treatment.

We first tested the effect of ENPP1 on tumor infiltrating dendritic cells. We knocked out ENPP1 in 4T1-Luc cells, validated the clones by their lack of enzymatic activity (commercially available ENPP1 antibodies are not sensitive enough to validate knockout), and pooled multiple clones to minimize clonal effects (Extended Data Fig. 7b). After 4T1-Luc implantation, we treated tumors with a dose of 20 Gy IR to induce

cGAMP production and excised the tumors after 24 hours to analyze their tumor-associated leukocyte compositions. ENPP1$^{-/-}$ tumors have a larger tumor-associated CD11c$^{+}$ population than WT tumors (Fig. 6a and Extended Data Fig. 7c). We then tested the effect of ENPP1 on immune rejection of 4T1-Luc tumors. This is an aggressive tumor model that typically metastasizes into the lungs within two weeks of tumor implantation[33]. The initial tumor growth rate for ENPP1$^{-/-}$ tumors before they reached 100 mm$^3$ was the same as WT tumors, suggesting that the ENPP1$^{-/-}$ cells are not slow-growing compared to the WT (Extended Data Fig. 7d). However, the established ENPP1$^{-/-}$ tumors are less aggressive and more responsive to IR (Fig. 6b). Without IR, the adaptive immune checkpoint blocker anti-CTLA-4 does not synergize with ENPP1$^{-/-}$ in shrinking tumors (Extended Data Fig. 7e, f). Strikingly, when we used IR to induce cGAMP production, anti-CTLA-4 cured 40% of ENPP1$^{-/-}$ tumors, but none of the WT tumors (Fig. 6c). Direct intratumoral injection of extracellular cGAMP is more effective in ENPP1$^{-/-}$ tumors than in WT tumors, and synergized with IR to cure 30% of mice (Fig. 6d) without the presence of anti-CTLA-4. Together, ENPP1 dampens extracellular cGAMP and innate immune detection of 4T1-Luc tumors, and negatively affects their responses to IR and adaptive immune checkpoint blockade.

Our genetic results suggest that ENPP1 is a potential target for pharmacological inhibition. The ENPP1 inhibitor we developed, STF-1084, exhibits fast clearance when intratumorally injected. Without extensive studies of route of administration and the corresponding formulation optimization that pharmaceutical companies typically perform at a later stage of drug development, we asked whether STF-1084 has an effect in vivo.

We injected tumors with STF-1084 immediately after IR treatment and observed an increase in the tumor-associated $CD11c^+$ population after 24 hours (Fig. 7a and Extended Data Fig. 8). Remarkably, STF-1084 synergized with IR and anti-CTLA-4 to achieve a 10% cure rate (Fig. 7b). Finally, STF-1084 synergized with IR and cGAMP to shrink tumors, prolong survival, and achieve a 10% cure rate (Fig. 7c). Together, our results demonstrate that ENPP1 can be targeted pharmacologically to enhance innate immune recognition of cancer, and STF-1084 serves as a starting point for new classes of ENPP1 inhibitors.

## Discussion

Here we report direct evidence of cGAMP export. Cell–cell cGAMP transfer through gap junctions and viral particles has been demonstrated previously. We provide the first in vitro and in vivo evidence that cGAMP can travel through the extracellular space (Extended Data Fig. 9). We hypothesize that cGAMP export is a hallmark of cancer cells since all the cell lines we tested synthesize and export cGAMP without external stimulation. Since chromosomal instability and aberrant cytosolic dsDNA are already considered tumor intrinsic properties and tumor cells rarely inactivate cGAS[22], we reason that constant cGAMP production and export may also be properties intrinsic to tumor cells. Since no cytosolic cGAMP hydrolase has been identified and ENPP1 cannot degrade intracellular cGAMP, export is currently the only mechanism by which cGAMP is removed from the cytosol, and represents another way to turn off intracellular

STING signaling in addition to ubiquitin-mediated STING degradation[34]. This clearance mechanism, however, exposes cancer cells to immune detection.

Indeed, our results demonstrate that cGAMP exported by cancer cells is a danger signal detected by the immune system. It is well known that neoantigens from cancer cells are presented by APCs to cross prime cytotoxic $CD8^+$ T cells that eventually perform cancer-specific killing[7,17]. However, it is less understood how APCs initially detect cancer cells. It has been shown that immunogenic tumors release dsDNA as a danger signal to $CD11c^+$ dendritic cells, an important type of APCs[7,35]. In addition, one study showed that cancer cells respond to their own cytosolic dsDNA induced by radiation and produce IFNs as a danger signal[27]. A recent study showed that the catalytic activity of tumor cGAS correlates with tumor immunity in the B16 melanoma model in a host STING dependent manner[36], suggesting that cGAMP could be transferred from tumor cells to host cells, with unknown mechanism. Here, we provide direct evidence that cancer cells produce soluble extracellular cGAMP as a danger signal, which leads to increased numbers of dendritic cells in the tumor microenvironment (Extended Data Fig. 10). cGAMP export is an important mode of cGAMP communication among cells that are not physically connected, but are in close proximity. Unlike cytokines, cGAMP cannot travel long distance in the extracellular space without being degraded and/or diluted to below its effective concentrations. This property is shared with neurotransmitters and qualifies cGAMP as the first identified immunotransmitter.

Releasing cGAMP into the extracellular space is, therefore, the Achilles heel of cancers if they cannot clear it quickly. One question in the field was how loss of cGAMP production in one cell could benefit the whole tumor that is still producing cGAMP[36]. We demonstrate that ENPP1 negatively regulates extracellular cGAMP signaling in vitro and its downstream anti-cancer immune activation in mice. Because tumor-derived soluble cGAMP is freely diffusible, overexpression of ENPP1 on one cell surface could certainly clear cGAMP in the nearby microenvironment and provide fitness to its neighbors. In humans, ENPP1 expression levels in breast cancers have been correlated with drug resistance[32], bone metastases[30], and poor prognosis[31]. ENPP1 should be formally evaluated as an innate immune checkpoint that can be inhibited to fully realize the power of cancer immunotherapy.

References


1. Wu, J. *et al.* Cyclic GMP-AMP is an endogenous second messenger in innate immune signaling by cytosolic DNA. *Science (80-. ).* **339,** 826–30 (2013).
2. Sun, L., Wu, J., Du, F., Chen, X. & Chen, Z. J. Cyclic GMP-AMP Synthase Is a Cytosolic DNA Sensor That Activates the Type I Interferon Pathway. *Science (80-. ).* **339,** 786–791 (2013).
3. Li, X.-D. *et al.* Pivotal Roles of cGAS-cGAMP Signaling in Antiviral Defense and Immune Adjuvant Effects. *Science (80-. ).* **341,** 1390–1394 (2013).
4. Barber, G. N. STING: infection, inflammation and cancer. *Nat. Rev. Immunol.* **15,** 760–770 (2015).

5. Ishikawa, H., Ma, Z. & Barber, G. N. STING regulates intracellular DNA-mediated, type i interferon-dependent innate immunity. *Nature* **461,** 788–792 (2009).

6. Ahn, J., Gutman, D., Saijo, S. & Barber, G. N. STING manifests self DNA-dependent inflammatory disease. *Proc. Natl. Acad. Sci.* **109,** 19386–19391 (2012).

7. Woo, S. R. *et al.* STING-dependent cytosolic DNA sensing mediates innate immune recognition of immunogenic tumors. *Immunity* **41,** 830–842 (2014).

8. Ishikawa, H. & Barber, G. N. STING is an endoplasmic reticulum adaptor that facilitates innate immune signalling. *Nature* **455,** 674–8 (2008).

9. Ablasser, A. *et al.* Cell intrinsic immunity spreads to bystander cells via the intercellular transfer of cGAMP. *Nature* **503,** 530–4 (2013).

10. Patel, S. J., King, K. R., Casali, M. & Yarmush, M. L. DNA-triggered innate immune responses are propagated by gap junction communication. *Proc. Natl. Acad. Sci.* **106,** 12867–12872 (2009).

11. Patel, S. J. *et al.* Gap junction inhibition prevents drug-induced liver toxicity and fulminant hepatic failure. *Nat. Biotechnol.* **30,** 179–183 (2012).

12. Chen, Q. *et al.* Carcinoma-astrocyte gap junctions promote brain metastasis by cGAMP transfer. *Nature* **533,** 493–8 (2016).

13. Gentili, M. *et al.* Transmission of innate immune signaling by packaging of cGAMP in viral particles. *Science (80-. ).* **349,** 1232–1236 (2015).

14. Bridgeman, A. *et al.* Viruses transfer the antiviral second messenger cGAMP between cells. *Science (80-. ).* **349,** 1228–1232 (2015).

15. Li, L. *et al.* Hydrolysis of 2’3’-cGAMP by ENPP1 and design of nonhydrolyzable

analogs. *Nat. Chem. Biol.* **10,** 1043–8 (2014).

16. Gao, P. *et al.* Structure-function analysis of STING activation by c[G(2′,5′) pA(3′,5′)p] and targeting by antiviral DMXAA. *Cell* **154,** 748–762 (2013).
17. Corrales, L. *et al.* Direct Activation of STING in the Tumor Microenvironment Leads to Potent and Systemic Tumor Regression and Immunity. *Cell Rep.* **11,** 1018–1030 (2015).
18. Jønsson, K. L. *et al.* IFI16 is required for DNA sensing in human macrophages by promoting production and function of cGAMP. *Nat. Commun.* **8,** 1–17 (2017).
19. Gao, D. *et al.* Activation of cyclic GMP-AMP synthase by self-DNA causes autoimmune diseases. *Proc. Natl. Acad. Sci. U. S. A.* **112,** E5699-705 (2015).
20. Mackenzie, K. J. *et al.* cGAS surveillance of micronuclei links genome instability to innate immunity. *Nature* **548,** 461–465 (2017).
21. Harding, S. M. Mitotic progression following DNA damage enables pattern recognition within micronuclei. *Nature* **548,** 466–470 (2017).
22. Bakhoum, S. F. *et al.* Chromosomal instability drives metastasis through a cytosolic DNA response. *Nature* **553,** 467–472 (2018).
23. Zhao, Y. J., Lam, C. M. C. & Lee, H. C. The membrane-bound enzyme CD38 exists in two opposing orientations. *Sci. Signal.* **5,** ra67 (2012).
24. Patel, S. D. *et al.* Quinazolin-4-piperidin-4-methyl sulfamide PC-1 inhibitors: Alleviating hERG interactions through structure based design. *Bioorganic Med. Chem. Lett.* **19,** 3339–3343 (2009).
25. Shayhidin, E. E. *et al.* Quinazoline-4-piperidine sulfamides are specific inhibitors of human NPP1 and prevent pathological mineralization of valve interstitial cells.

*Br. J. Pharmacol.* **172,** 4189–4199 (2015).

26. Bakhoum, S. F. *et al.* Numerical chromosomal instability mediates susceptibility to radiation treatment. *Nat. Commun.* **6,** 1–10 (2015).
27. Vanpouille-Box, C. *et al.* DNA exonuclease Trex1 regulates radiotherapy-induced tumour immunogenicity. *Nat. Commun.* **8,** 15618 (2017).
28. Zhang, H. & Verkman, A. S. Microfiberoptic measurement of extracellular space volume in brain and tumor slices based on fluorescent dye partitioning. *Biophys. J.* **99,** 1284–1291 (2010).
29. We use 1 mL of culture media per 1 x $10^6$ cells and estimate a cell volume of ~1-4 pL to perform this calculation.
30. Lau, W. M. *et al.* Enpp1: A Potential Facilitator of Breast Cancer Bone Metastasis. *PLoS One* **8,** 1–5 (2013).
31. Takahashi, R. U. *et al.* Loss of microRNA-27b contributes to breast cancer stem cell generation by activating ENPP1. *Nat. Commun.* **6,** 1–15 (2015).
32. Umar, A. *et al.* Identification of a Putative Protein Profile Associated with Tamoxifen Therapy Resistance in Breast Cancer. *Mol. Cell. Proteomics* **8,** 1278–1294 (2009).
33. Pulaski, B. A. & Ostrand-Rosenberg, S. Reduction of Established Spontaneous Mammary Carcinoma Metastases following Immunotherapy with Major Histocompatibility Complex Class II and B7.1 Cell-based Tumor Vaccines. *Cancer Res.* **58,** 1486–1493 (1998).
34. Konno, H., Konno, K. & Barber, G. N. Cyclic dinucleotides trigger ULK1 (ATG1) phosphorylation of STING to prevent sustained innate immune signaling. *Cell*

**155,** 688–698 (2013).

35. Xu, M. M. *et al.* Dendritic Cells but Not Macrophages Sense Tumor Mitochondrial DNA for Cross-priming through Signal Regulatory Protein a Signaling. *Immunity* **47,** 363–373 (2017).

36. Marcus, A. *et al.* Tumor-Derived cGAMP Triggers a STING-Mediated Interferon Response in Non-tumor Cells to Activate the NK Cell Response. *Immunity* **49,** 754–763.e4 (2018).

37. Sanjana, N. E., Shalem, O. & Zhang, F. Improved vectors and genome-wide libraries for CRISPR screening. *Nat. Methods* **11,** 783–784 (2014).

38. Vilalta, M., Rafat, M., Giaccia, A. J. & Graves, E. E. Recruitment of Circulating Breast Cancer Cells Is Stimulated by Radiotherapy. *Cell Rep.* **8,** 402–409 (2014).

39. Kato, K. *et al.* Expression, purification, crystallization and preliminary X-ray crystallographic analysis of Enpp1. *Acta Crystallogr. Sect. F Struct. Biol. Cryst. Commun.* **68,** 778–782 (2012).

40. Kato, K. *et al.* Crystal structure of Enpp1, an extracellular glycoprotein involved in bone mineralization and insulin signaling. *Proc. Natl. Acad. Sci. U. S. A.* **109,** 16876–81 (2012).

**Acknowledgments:**

This work is dedicated to Dr. T. Mitchison to celebrate his 60$^{th}$ birthday and his remarkable achievements in understanding biochemical mechanisms of the cell. He taught Dr. L. Li the power of definitive experiments. We thank the following insitutions and people for their help: Stanford Small Animal Imaging Facility, S. Ergun for $^{35}$S

cGAMP, C. Patel for specificity assays, F. Sunden for enzyme assays, R. Stabler for chemical synthesis, N. Weng for protein purification, Dr. C. Walsh, Dr. D. Herschlag, and all members of the Li lab for helpful discussions. Flow cytometry analysis for this project was done on instruments in the Stanford Shared FACS Facility. Data was collected on an instrument in the Shared FACS Facility obtained using NIH S10 Shared Instrument Grant S10RR027431-01. **Funding:** This research was supported by the National Institutes of Health grant DP2CA228044 (L.L.), DOD grant W81XWH-18-1-0041 (L.L.), U19AI109662 (J.S.G.), R01CA197136 and S10OD018208 (E.E.G.), and K99CA201304 (M.R.). J.A.C. thanks the Stanford Interdisciplinary Graduate Fellowship affiliated with Stanford ChEM-H. **Author Contributions:** J.A.C., V.B., K.E.S., M.S., and L.L. designed the study. J.A.C., V.B., K.E.S., K.N., G.S., J.A.B., M.R., and L.L. performed experiments and analyzed data. R.E. performed statistical analysis. J.A.C., V.B., and L.L. wrote the manuscript. J.S.G. supervised K.N.; E.E.G. supervised M.R. All authors discussed the findings and commented on the manuscript. **Competing interests:** The authors declare no competing financial interests. **Data and materials availability:** All data are available in the main text or supplementary information.

## Figures

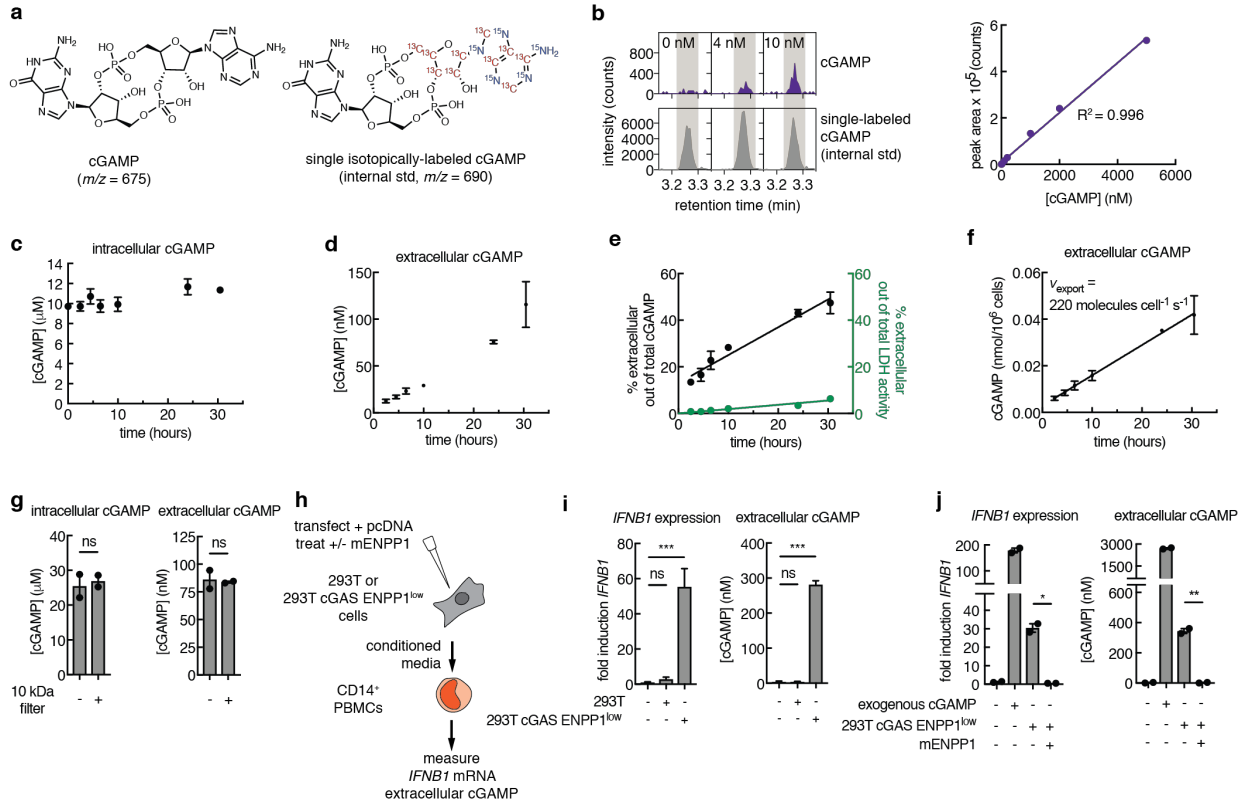


**Figure 1 | cGAMP is exported from 293T cGAS ENPP1$^{-/-}$ cells as a soluble factor.**

**a**, Chemical structures of cGAMP and single isotopically-labeled cGAMP.

**b**, cGAMP is detected by LC-MS/MS, lower limit of quantification = 4 nM. (left) Liquid chromatography traces of cGAMP at 0, 4, and 10 nM and single isotopically-labeled cGAMP (15 Da heavier) at 500 nM as an internal standard; (right) external standard curve of cGAMP, $R^2$ = 0.996. Data are representative of > 10 independent experiments.

**c-d**, Intracellular and extracellular concentrations of cGAMP from 293T cGAS ENPP1$^{-/-}$ cells without exogenous stimulation measured using LC-MS/MS. At time 0, cells were

replenished with serum-free media. Mean ± SEM (*n* = 2) with some error bars too small to visualize. Data are representative of three independent experiments.

**e**, The fraction of extracellular/total cGAMP molecules (left y-axis) calculated from data in (**c**) and (**d**) compared to the fraction of extracellular/total lactose dehydrogenate (LDH) activity (right y-axis).

**f**, The amount of cGAMP exported per cell over time calculated from data in (**d**). The export rate was found using linear regression.

**g**, Intracellular and extracellular cGAMP concentrations produced by 293T cGAS ENPP1$^{-/-}$ cells measured before and after passing the media through 10 kDa filters. Mean ± SEM (*n* = 2). Data are representative of two independent experiments.

**h**, Schematic of the conditioned media transfer experiment for (**i**) and (**j**). cGAS-null 293T or 293T cGAS ENPP1$^{low}$ cells were transfected with empty pcDNA vector and treated +/- 20 nM recombinant mouse ENPP1 (mENPP1). Conditioned media from these cells was transferred to primary CD14$^{+}$ human PBMCs.

**i**, *IFNB1* mRNA levels were normalized to *CD14* and the fold induction was calculated relative to untreated CD14$^{+}$ cells. Mean ± SEM (*n* = 4). ***$P$ = 0.0003 (one-way ANOVA). cGAMP concentrations were measured in the conditioned media by LC-MS/MS. Mean ± SEM (*n* = 2). ***$P$ = 0.0002 (one-way ANOVA). Data are representative of two independent experiments.

**j**, *IFNB1* mRNA levels were normalized to *CD14* and the fold induction was calculated relative to untreated CD14$^{+}$ cells. Mean ± SEM (*n* = 2). *$P$ = 0.04 (one-way ANOVA). cGAMP concentrations were measured in the conditioned media by LC-MS/MS. Mean ±

SEM ($n$ = 2). **$P$ = 0.002 (one-way ANOVA). Data are representative of two independent experiments.

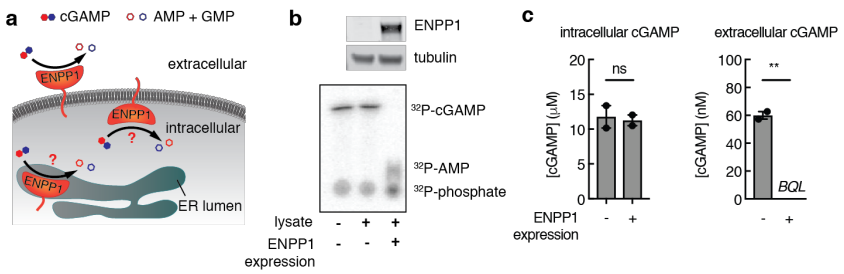


**Figure 2 | ENPP1 only regulates extracellular cGAMP.**

**a**, Three possible cellular locations of ENPP1 activity.

**b**, 293T cGAS ENPP1$^{-/-}$ cells were transfected with empty vector or vector containing human *ENPP1* and analyzed after 24 h for ENPP1 protein expression using western blot (top) and for ENPP1 $^{32}$P-cGAMP hydrolysis activity using thin layer chromatography (TLC) (bottom). Data are representative of two independent experiments.

**c**, Intracellular and extracellular cGAMP concentrations measured using LC-MS/MS. *BQL* = below quantification limit. Mean ± SEM ($n$ = 2). $^{**}P$ = 0.002 (Student's $t$ test). Data are representative of three independent experiments.

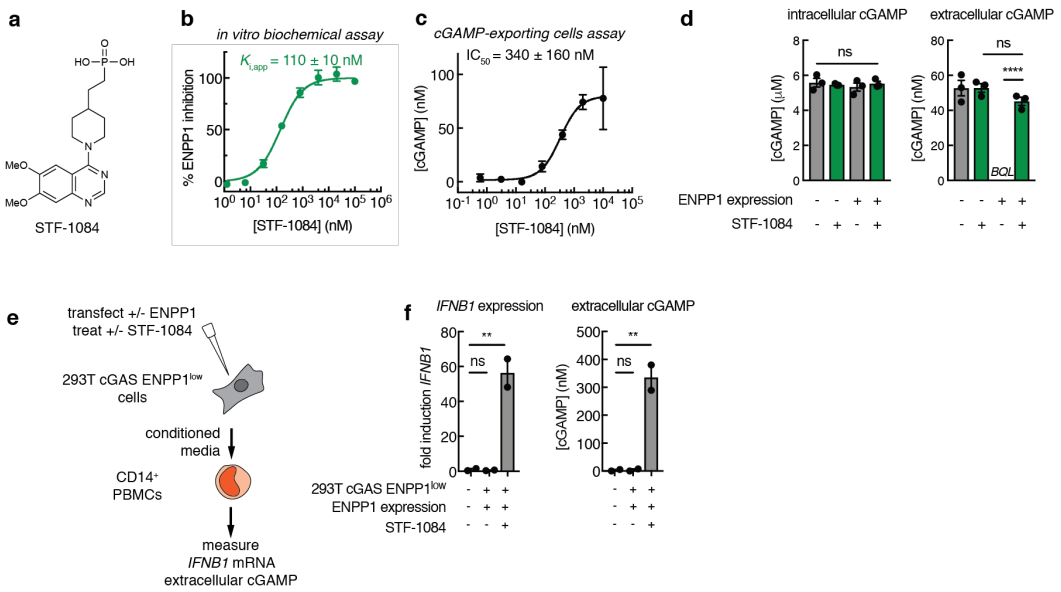


**Figure 3 | Development of a cell impermeable ENPP1 inhibitor.**

**a**, Chemical structure of STF-1084.

**b**, Inhibitory activity of STF-1084 against purified mouse ENPP1 with $^{32}$P-cGAMP as the substrate at pH 7.5 ($K_{i,app}$ = 110 ± 10 nM). Mean ± SEM (*n* = 3 independent experiments) with some error bars too small to visualize.

**c**, Inhibitory activity of STF-1084 against human ENPP1 transiently expressed in 293T cGAS ENPP1$^{-/-}$ cells ($IC_{50}$ = 340 ± 160 nM). Extracellular cGAMP levels were analyzed by LC-MS/MS after 24 hours. Mean ± SEM (*n* = 2).

**d**, Intracellular and extracellular cGAMP concentrations for 293T cGAS ENPP1$^{-/-}$ cells transfected with empty pcDNA vector or vector containing human *ENPP1* in the presence or absence of 10 μM STF-1084 after 24 hours. cGAMP levels were analyzed by LC-MS/MS. *BQL* = below quantification limit. Mean ± SEM (*n* = 3). ****$P$ < 0.0001 (one-way ANOVA). Data are representative of two independent experiments.

**e**, Schematic of the conditioned media experiment. 293T cGAS ENPP1$^{low}$ cells were transfected with vector containing human *ENPP1* and incubated in the presence or absence of STF-1084. Conditioned media from these cells was transferred to primary CD14$^{+}$ human PBMCs.

**f**, *IFNB1* mRNA levels were normalized to *CD14* and the fold induction was calculated relative to untreated CD14$^{+}$ cells. Mean ± SEM ($n$ = 2). **$P$ = 0.007 (one-way ANOVA). cGAMP concentrations were measured in the conditioned media by LC-MS/MS. Mean ± SEM ($n$ = 2). **$P$ = 0.006 (one-way ANOVA). Data are representative of two independent experiments.

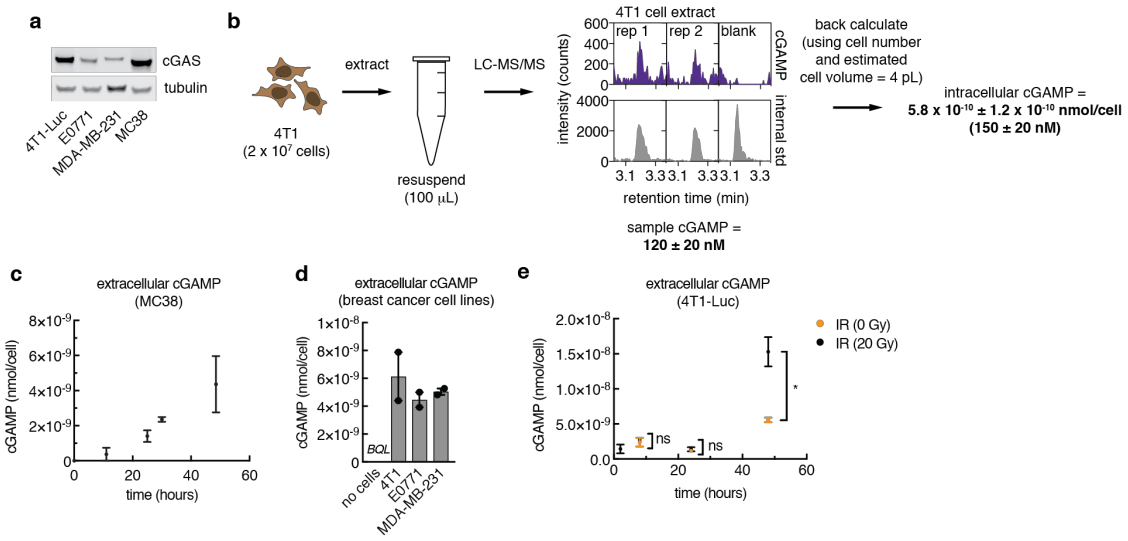


**Figure 4 | Cancer cells express cGAS and continuously export cGAMP in culture.**

**a**, cGAS expression of 4T1-Luc, E0771, MDA-MB-231, and MC38 analyzed by western blot.

**b**, Estimate of the concentration of intracellular cGAMP in 4T1-Luc cells without exogenous stimulation. Mean ± SEM (*n* = 2).

**c**, Extracellular cGAMP produced by MC38 cells over 48 hours. At time 0, cells were refreshed with media supplemented with 50 μM STF-1084. Mean ± SEM (*n* = 2). Data are representative of two independent experiments.

**d**, Extracellular cGAMP produced by 4T1-Luc, E0771, and MDA-MB-231 cells measured after 48 h in the presence of 50 μM STF-1084. *BQL* = below quantification limit. Mean ± SEM (*n* = 2).

**e**, Extracellular cGAMP produced by 4T1-Luc cells over 48 hours. At time 0, cells were left untreated or treated with 20 Gy IR and refreshed with media supplemented with 50 μM STF-1084. Mean ± SEM (*n* = 2). *$P$ = 0.04 (Student's *t* test).

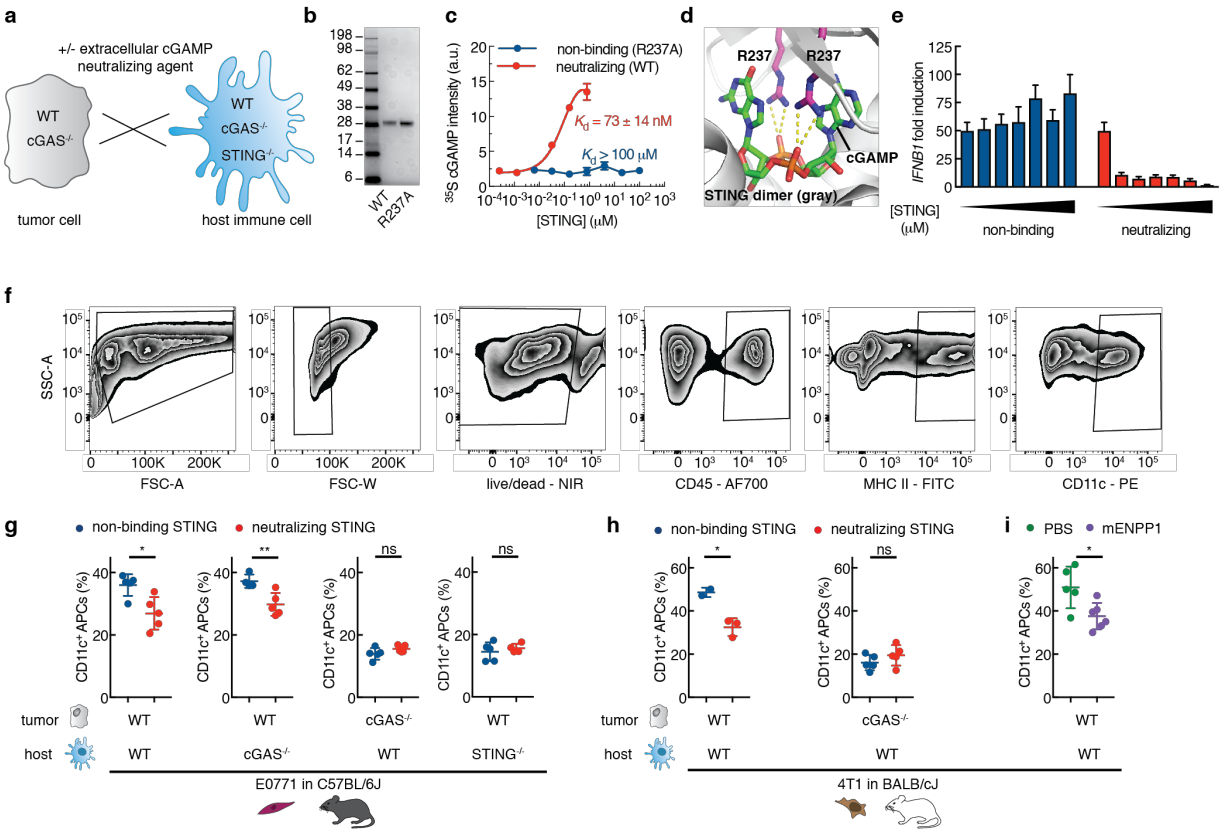


**Figure 5 | Sequestration of extracellular cGAMP decreases tumor-associated dendritic cells in a tumor cGAS and host STING dependent manner.**

**a**, Experimental setup to assess the role of extracellular cGAMP in vivo.

**b**, Coomassie gel of recombinant mouse WT STING and R237A STING.

**c**, Binding curves for the cytosolic domain of mouse WT STING (neutralizing) and R237A STING (non-binding) determined by a membrane binding assay using radiolabeled $^{35}$S-cGAMP as the probe. Mean ± SEM ($n$ = 2 from two independent experiments).

**d**, Crystal structure of mouse WT STING in complex with cGAMP with R237 highlighted in pink (PDB ID 4LOJ).

**e**, *IFNB1* mRNA fold induction in $CD14^+$ PBMCs treated with 2 μM cGAMP in the presence of neutralizing or non-binding STING (2 μM to 100 μM, 2.5-fold dilutions). Mean ± SEM (*n* = 2 technical qPCR replicates).

**f**, WT or $cGAS^{-/-}$ E0771 cells ($1x10^6$) were orthotopically injected into WT, $cGAS^{-/-}$, or $STING^{-/-}$ C57BL/6J mice on day 0. Neutralizing (WT mice *n* = 5; $cGAS^{-/-}$ mice *n* = 5; $STING^{-/-}$ mice *n* = 4) or non-binding STING (WT mice *n* = 5; $cGAS^{-/-}$ mice *n* = 4; $STING^{-/-}$ mice *n* = 5) was intratumorally injected on day 2. Tumors were harvested and analyzed by FACS on day 3. Samples were gated on cells in FSC-A/SSC-A, singlets (FSC-W), living cells, $CD45^+$, MHC $II^+$, $CD11c^+$ populations.

**g**, Percent $CD11c^+$ cells of total APCs. Mean ± SD. **P* = 0.015. ***P* = 0.008 (Welch's *t* test).

**h**, The same procedure was performed as in (**f**) and (**g**) with WT (neutralizing STING *n* = 3; non-binding STING *n* = 2) or $cGAS^{-/-}$ 4T1-Luc cells (*n* = 5) in WT BALB/cJ mice. Mean ± SD. **P* = 0.011. (Welch's *t* test).

**i**, 4T1-Luc cells ($1x10^6$) were orthotopically injected into WT BALB/cJ mice on day 0. PBS (*n* = 5) or recombinant mouse ENPP1 (mENPP1) (*n* = 6) was intratumorally injected on day 2. Tumors were harvested and analyzed by FACS on day 3. Mean ± SD. **P* = 0.033. (Welch's *t* test).

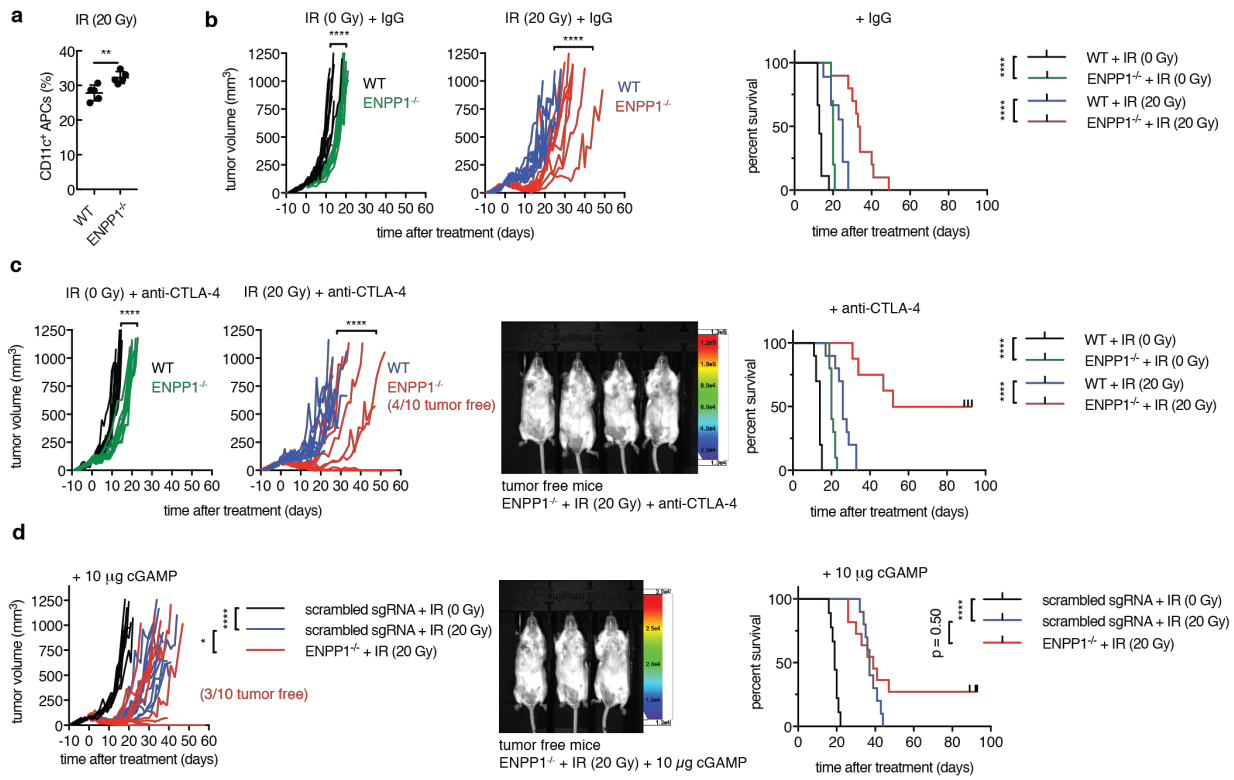


**Figure 6 | ENPP1$^{-/-}$ tumors have increased innate immune infiltration, are less aggressive, and are more susceptible to IR and anti-CTLA-4 therapy.**

**a**, WT or ENPP1$^{-/-}$ 4T1-Luc cells (1x10$^6$) were orthotopically injected into WT BALB/cJ mice on day 0 ($n$ = 5 for each group) Tumors were treated with IR at 20 Gy on day 2. Tumors were harvested and analyzed by FACS on day 3. Multiple ENPP1$^{-/-}$ 4T1-Luc cell clones were pooled before injection to minimize clonal effects. **$P$ = 0.008 (Welch's $t$ test).

**b**, Established WT or ENPP1$^{-/-}$ 4T1-Luc tumors (100 ± 20 mm$^3$) were treated once with 0 Gy or 20 Gy IR followed by three intraperitoneal injections of IgG on day 2, 5, and 7 after IR. ($n$ = 9 for WT 4T1-Luc, $n$ = 10 for ENPP1$^{-/-}$ 4T1-Luc). Tumor volumes and Kaplan Meier curves are shown. $P$ values determined by pairwise comparisons using

post hoc tests with a Tukey adjustment at day 20 (tumor volumes) and the log-rank Mantel-Cox test (Kaplan Meier). ****$P < 0.0001$.

**c**, Established WT or ENPP1$^{-/-}$ 4T1-Luc tumors (100 ± 20 mm$^3$) were treated once with 0 Gy or 20 Gy IR followed by three intraperitoneal injections of anti-CTLA-4 on day 2, 5, and 7 after IR ($n$ = 10 for all groups). Tumor volumes and Kaplan Meier curves are shown. $P$ values determined by pairwise comparisons using post hoc tests with a Tukey adjustment at day 20 (tumor volumes) and the log-rank Mantel-Cox test (Kaplan Meier). ****$P < 0.0001$. In the ENPP1$^{-/-}$ 4T1-Luc + IR (20 Gy) + anti-CTLA-4 treatment group, 4/10 (40%) mice are tumor-free survivors verified by bioluminescent imaging.

**d**, Established 4T1-Luc tumors infected with a scrambled sgRNA sequence or ENPP1$^{-/-}$ 4T1-Luc tumors (100 ± 20 mm$^3$) were treated once with 20 Gy IR followed by three intratumoral injections of 10 µg cGAMP on day 2, 4, and 7 after IR ($n$ = 10 for both groups). Tumor volumes and Kaplan Meier curves are shown. $P$ values determined by pairwise comparisons using post hoc tests with a Tukey adjustment at day 20 (tumor volumes) and the log-rank Mantel-Cox test (Kaplan Meier). *$P < 0.05$, ****$P < 0.0001$. In the ENPP1$^{-/-}$ 4T1-Luc + IR (20 Gy) cGAMP treatment group, 3/10 (30%) mice are tumor-free survivors verified by bioluminescent imaging.

Mice from different treatment groups in **b-d** were co-housed and the experimenter was blinded.

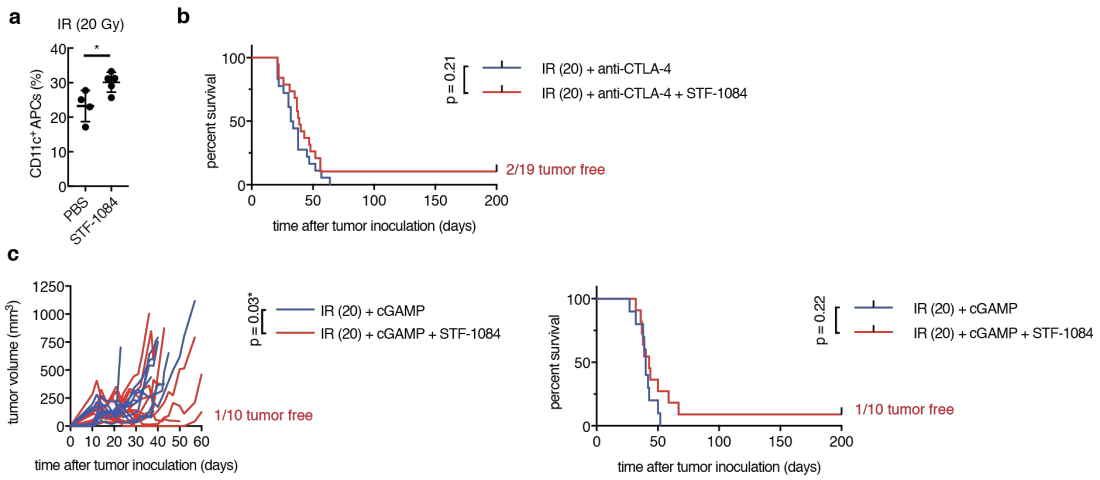


**Figure 7 | ENPP1 inhibition synergizes with IR treatment and anti-CTLA-4 to exert anti-tumor effects.**

**a**, 4T1-Luc cells ($1x10^6$) were orthotopically injected into WT BALB/cJ mice on day 0. Tumors were treated with 20 Gy IR and intratumorally injected with PBS (*n* = 4) or STF-1084 (*n* = 5) on day 2. Tumors were harvested and analyzed by FACS on day 3. **P* = 0.047 (Welch's *t* test).

**b**, Established 4T1-Luc tumors (100 ± 20 $mm^3$) were treated once with 20 Gy IR followed by three intratumoral injections of PBS or STF-1084 on day 2, 4, and 7 and intraperitoneal injections of anti-CTLA-4 or on days 2, 5, and 7 (*n* = 17-19 for all treatment groups). Tumor volumes and Kaplan Meier curves are shown. *P* values determined by pairwise comparisons using post hoc tests with a Tukey adjustment at day 40 (tumor volumes) and the log-rank Mantel-Cox test (Kaplan Meier).

**c**, Established 4T1-Luc tumors (100 ± 20 $mm^3$) were treated once with 20 Gy IR followed by three intratumoral injections of cGAMP alone or cGAMP + STF-1084 on day 2, 4, and 7 after IR (*n* = 9 per treatment group). Tumor volumes and Kaplan Meier

curves are shown. *P* values determined by pairwise comparisons using post hoc tests with a Tukey adjustment at day 40 (tumor volumes) and the log-rank Mantel-Cox test (Kaplan Meier).

**Materials and Methods:**

Reagents, antibodies, and cell lines

[$\alpha$-$^{32}$P]ATP (800 Ci/mmol, 10 mCi/mL, 250 $\mu$Ci) and [$^{35}$S]ATP$\alpha$S (1250 Ci/mmol, 12.5 mCi/mL, 250 $\mu$Ci) were purchased from Perkin Elmer. Adenosine triphosphate, guanosine triphosphate, adenosine-$^{13}C_{10}$,$^{15}N_5$, 5'-triphosphate, guanosine-$^{13}C_{10}$,$^{15}N_5$-triphosphate, 4-nitrophenyl phosphate, and bis(4-nitrophenyl) phosphate were purchased from Sigma-Aldrich and are >98% atomically pure. 2'3'-cGAMP was purchased from Invivogen. Caco-2 assay was purchased from Cyprotex. Kinome screens were conducted by Eurofins. PAMPA and MDCK permeability assays were conducted by Quintara Discovery. Total protein content was quantified using the BCA assay (ThermoFisher). Cell viability was quantified using the CellTiterGlo assay (Promega). Full length human *ENPP1* was cloned into pcDNA3 vector. A set of 4 ON-TARGETplus ENPP1 siRNA (LQ-003809-00-0002) were purchased from Dharmacon. QS1 was synthesized as previously described [25]. The following monoclonal antibodies were used for western blotting: rabbit anti-cGAS (D1D3G Cell Signaling, 1:1,000) rabbit anti-mouse cGAS (D2O8O Cell Signaling, 1:1,000), mouse anti-tubulin (DM1A Cell Signaling, 1:2,000), and rabbit anti-STING (D2P2F Cell Signaling, 1:1,000), IRDye 800CW goat anti-rabbit (LI-COR, 1:15,000), and IRDye 680RD goat anti-mouse (LI-COR, 1:15,000).

293T cells were purchased from ATCC and viral transfected to stably express mouse cGAS. 293T cGAS ENPP1$^{low}$ cells were created by viral transfection of CRISPR sgRNA targeting human *ENPP1* (5'-CACCGCTGGTTCTATGCACGTCTCC-3'), and 293T

mcGAS ENPP1$^{-/-}$ cells were selected after single cell cloning from this pool. 4T1 and E0771 *cGAS*$^{-/-}$ cells were created by viral transfection of CRISPR sgRNA (using lentiCRISPRv2-blast, Addgene plasmid #83480) targeting mouse *Mb21d1* (5'-CACCGGAAGGGGCGCGCGCTCCACC-3'). Cells were selected after single cell cloning. 4T1-Luc ENPP1$^{-/-}$ cells were created by viral transfection of CRISPR sgRNAs (using lentiCRISPRv2-blast)[37] targeting mouse *Enpp1* (5'- GCTCGCGCCCATGGACCT-3' and 5'- ATATGACTGTACCCTACGGG -3') or a scrambled sequence. 4T1-Luc shcGAS cells were created by viral transfection of shRNA (5'-CAGGATTGAGCTACAAGAATAT-3') using the plasmid pGH188. Cells harboring the shRNA were selected with blasticidin and sorted for GFP expression, and were used as a pool for experiments. MDA-MB-231 were purchased from ATCC, E0771 were purchased from CH3 BioSystems, 4T1-luciferase were a gift from Dr. Christopher Contag[38], and HEK293S GnT1$^{-}$ cells expressing secreted mENPP1 were a gift from Dr. Osamu Nureki[39].

Cell culture

Cell lines were maintained in DMEM (Corning Cellgro) (293T, MC38) or RPMI (Corning Cellgro) (4T1-Luc, E0771, MDA-MD-231) supplemented with 10% FBS (Atlanta Biologics) (v/v) and 100 U/mL penicillin-streptomycin (ThermoFisher). Primary human peripheral blood mononuclear cells (PBMCs) were isolated by subjecting enriched buffy coat from whole blood to a Percoll density gradient. CD14$^{+}$ PBMCs were isolated using CD14$^{+}$ MicroBeads (Miltenyi). CD14$^{+}$ PBMCs were cultured in RMPI supplemented with 2% human serum and 100 U/mL penicillin-streptomycin.

Expression and purification of recombinant proteins

sscGAS: The DNA sequence encoding porcine cGAS (residues 135-497) was amplified from a porcine cDNA library using the primer pair fwd: (5'-CTGGAAGTTCTGTTCCAGGGGCCCCATATGGGCGCCTGGAAGCTCCAGAC-3') and rev: (5'-GATCTCAGTGGTGGTGGTGGTGGTGCTCGAGCCAAAAAACTGGAAATCCATTGT-3'). The PCR product was inserted into pDB-His-MBP (a generous gift from Qian Yin, Florida State University) via Gibson assembly and expressed in Rosetta cells. Cells were grown in 2xYT medium with kanamycin (100 µg/ml), induced with 0.5 mM IPTG when the $OD_{600}$ reached 1, and were allowed to grow overnight at 16 °C. All following procedures involving proteins and cell lysates were conducted at 4 °C. Cells were pelleted and lysed in 20 mM HEPES pH 7.5, 400 mM NaCl, 10% glycerol, 10 mM imidazole, 1 mM DTT, and protease inhibitor cocktail (cOmplete EDTA free tablets, Roche). The cell extract was cleared by ultracentrifugation at 50,000 x g for 1 h. The cleared supernatant was incubated with HisPur Cobalt resin (ThermoFisher Scientific; 1 mL resin per liter of bacteria culture). Cobalt resin was washed with 20 mM HEPES pH 7.5, 1 M NaCl, 10% glycerol, 10 mM imidazole, 1 mM DTT. Protein was eluted from resin with 300 mM imidazole in 20 mM HEPES pH 7.5, 1 M NaCl, 10% glycerol, and 1 mM DTT. Fractions containing His-MBP-sscGAS were pooled, concentrated and dialyzed against 20 mM HEPES pH 7.5, 400 mM NaCl, 1 mM DTT. The protein was snap frozen in aliquots for future use.

STING: Mouse STING (residues 139-378) was inserted into the pTB146 His-SUMO vector (a generous gift from T. Bernhard, Harvard Medical School) and expressed in Rosetta cells. Cells were grown in 2xYT medium with 100 µg/mL ampicillin and induced when the $OD_{600}$ reached 1 with 0.75 mM IPTG at 16 °C overnight. All subsequent procedures using proteins and cell lysates were performed at 4 °C. Cells were pelleted and lysed in 50 mM Tris pH 7.5, 400 mM NaCl, 10 mM imidazole, 2 mM DTT, and protease inhibitors (cOmplete, EDTA-free protease inhibitor cocktail Roche). Cells were lysed by sonication and the lysate was cleared by ultracentrifugation at 50,000 rcf for 1 hour. The cleared supernatant was incubated with HisPur cobalt resin (ThermoFisher Scientific; 1 mL resin per 1 L bacterial culture) for 30 minutes. The resin-bound protein was washed with 50 column volumes of 50 mM Tris pH 7.5, 150 mM NaCl, 2% triton X-114, 50 CV of 50 mM Tris pH 7.5, 1 M NaCl (each wash was set to a drip rate of 1 drop/2-3 seconds and took 2-3 hours), and 20 CV of 50 mM Tris pH 7.5, 150 mM NaCl. Protein was eluted from resin with 600 mM imidazole in 50 mM Tris pH 7.5, 150 mM NaCl. Fractions containing His-SUMO-STING were pooled, concentrated, and dialyzed against 50 mM Tris pH 7.5, 150 mM NaCl while incubating with the SUMOlase enzyme His-ULP1 to remove the His-SUMO tag overnight. The solution was incubated with the HisPur cobalt resin again to remove the His-SUMO tag, and STING was collected from the flowthrough. Protein was dialyzed against 50 mM Tris pH 7.5, loaded onto a HitrapQ anion exchange column (GE Healthcare) using an Äkta FPLC (GE Healthcare), and eluted with a NaCl gradient. Fractions containing STING were pooled and buffer exchanged into PBS and stored at 4 °C until use.

ENPP1: mENPP1 was produced as described previously[39,40].

Liquid chromatography-tandem mass spectrometry

Cyclic GMP-$^{13}C_{10}$,$^{15}N_5$-AMP was used as an internal standard and cyclic $^{13}C_{10}$,$^{15}{}_5$-GMP-$^{13}C_{10}$,$^{15}N_5$-AMP was used as an extraction standard. Isotope-labeled cGAMP standards were synthesized by incubating 1 mM ATP (isotope labeled), 1 mM GTP (isotope labeled), 20 mM $MgCl_2$, 0.1 mg/mL herring testes DNA (Sigma), and 2 μM sscGAS in 100 mM Tris, pH 7.5 overnight. The reaction was heated at 95°C and filtered through a 3 kDa centrifuge filter. Water was removed on a rotary evaporator. cGAMP was purified from the crude reaction mixture using a PLRP-S polymeric reversed phase preparatory column (100 Å, 8 μm, 300 x 25 mm; Agilent Technologies) on a preparatory HPLC (1260 Infinity LC system; Agilent Technologies) connected to UV-vis detector (ProStar; Agilent Technologies) and fraction collector (440-LC; Agilent Technologies). The flow rate was set to 25 mL/min. The mobile phase consisted of 10 mM triethylammonium acetate in water and acetonitrile. The mobile phase started as 2% acetonitrile for the first 5 min. Acetonitrile was then ramped up to 30% from 5-20 min, ramped up to 90% from 20-22 min, maintained at 90% from 22-25 min, and then ramped down to 2% from 25-28 min. Fractions containing cGAMP were lyophilized and resuspended in water. The concentration was determined by measuring absorbance at 280 nm. Samples were analyzed for cGAMP, ATP, and GTP content on a Shimadzu HPLC (San Francisco, CA) with an autosampler set at 4°C and connected to an AB Sciex 4000 QTRAP (Foster City, CA). A volume of 10 μL was injected onto a Biobasic AX LC column, 5 μm, 50 x 3 mm (Thermo Scientific). The mobile phase consisted of 100 mM ammonium carbonate

(A) and 0.1% formic acid in acetonitrile (B). Initial condition was 90% B, maintained for 0.5 min. The mobile phase was ramped to 30% A from 0.5 min to 2.0 min, maintained at 30% A from 2.0 min to 3.5 min, ramped to 90% B from 3.5 min to 3.6 min, and maintained at 90% B from 3.6 min to 5 min. The flow rate was set to 0.6 mL/min. The mass spectrometer was operated in electrode spray positive ion mode with the source temperature set at 500°C. Declustering and collision-induced dissociation were achieved using nitrogen gas. Declustering potential and collision energy were optimized by direct infusion of standards. For each molecule, the MRM transition(s) (*m/z*), DP (V), and CE (V) are as follows: ATP (508 > 136, 341, 55), GTP (524 > 152, 236, 43), cGAMP (675 > 136, 121, 97; 675 > 312, 121, 59; 675 > 152, 121, 73), internal standard cyclic GMP-$^{13}C_{10}$,$^{15}N_5$-AMP (690 > 146, 111, 101; 690 > 152, 111, 45; 690 > 327, 111, 47), extraction standard cyclic $^{13}C_{10}$,$^{15}N_5$-GMP-$^{13}C_{10}$,$^{15}N_5$-AMP (705 > 156, 66, 93; 705 > 162, 66, 73).

Export assay in 293T cGAS ENPP1$^{-/-}$ cells

293T cGAS ENPP1$^{-/-}$ cells were plated in tissue culture treated plates coated with PurCol (Advanced BioMatrix). 24 hours later, the media was gently removed and replaced with serum-free DMEM supplemented with 1% insulin-transferrin-selenium-sodium pyruvate (ThermoFisher) and 100 U/mL penicillin-streptomycin. At indicated times, the media was removed and the cells were washed off the plate with cold PBS. Both the media and cells were centrifuged at 1000 rcf for 10 minutes at 4 °C. The cells were lysed in 30 to 100 μL of 50:50 acetonitrile:water supplemented with 500 nM internal standard, and centrifuged at 15,000 rcf for 20 minutes at 4 °C to remove the

insoluble fraction. If no concentration was necessary, an aliquot of media was removed, supplemented with internal standard at 500 nM and 20% formic acid. If concentration was necessary, the media was acidified with 0.5% acetic acid and supplemented with extraction standard (the appropriate amount for a final concentration of 2 μM in 100 μL). Media was applied to HyperSep Aminopropyl SPE columns (ThermoFisher Scientific) to enrich for cGAMP as described previously[19]. Eluents were evaporated to dryness and reconstituted in 50:50 acetonitrile:water supplemented with 500 nM internal standard. The media and cell extract were submitted for mass spectrometry quantification of cGAMP, ATP, and GTP.

Transfection stimulation of 293T cGAS ENPP1$^{-/-}$ cells

293T cGAS ENPP1$^{-/-}$ cells were transfected with Fugene 6 (Promega) according to manufacturer's instructions plus indicated concentrations of pcDNA3 plasmid DNA (empty or containing human *ENPP1*). 24 hours following transfection, the export assay was conducted as described above.

Conditioned media transfer

293T cGAS ENPP1$^{low}$ cells were plated and transfected with plasmid DNA as described above. 24 hours following transfection, media was changed to RPMI + 2% human serum + 1% penicillin-streptomycin, +/- 2 μM cGAMP, +/- 20 nM recombinant mENPP1, or +/- 50 uM STF-1084. 24 hours following media change, the conditioned media was removed from the 293T cGAS ENPP1$^{low}$ cells and incubated with freshly isolated CD14$^{+}$ PBMCs. Gene expression of CD14$^{+}$ PBMCs was analyzed 14-16 h later.

RT-PCR analysis

Total RNA was extracted using Trizol (Thermo Fisher Scientific) and reverse transcribed with Maxima H Minus Reverse Transcriptase (Thermo Fisher Scientific). Real-time RT-PCR was performed in duplicate with AccuPower 2X Greenstar qPCR Master Mix (Bioneer) on a 7900HT Fast Real-Time PCR System (Applied Biosystems). Data were normalized to *CD14*, *ACTB*, or *GAPDH* expression for each sample. Fold induction was calculated using ΔΔCt. Primers for human *IFNB1*: fwd (5'-AAACTCATGAGCAGTCTGCA-3'), rev (5'-AGGAGATCTTCAGTTTCGGAGG-3'); human *CD14*: fwd (5'-GCCTTCCGTGTCCCCACTGC-3'), rev (5'-TGAGGGGGCCCTCGACG-3'); human *ACTB*: fwd (5'-GGCATCCTCACCCTGAAGTA-3'), rev (5'- AGAGGCGTACAGGGATAGCA-3'); human *GAPDH*: fwd (5'-CCAAGGTCATCCATGACAAC-3'); rev (5'-CAGTGAGCTTCCCGTTCAG-3').

$^{32}$P-cGAMP degradation TLC assay

Radiolabeled $^{32}$P cGAMP was synthesized by incubating unlabeled ATP (1 mM) and GTP (1 mM) doped with $^{32}$P-ATP with 2 μM purified recombinant porcine cGAS in 20 mM Tris pH 7.5, 2 mM $MgCl_2$, 100 μg/mL herring testes DNA) overnight at room temperature, and the remaining nucleotide starting materials were degraded with alkaline phosphatase for 4 h at 37 °C. Cell lysates were generated by scraping and lysing $1x10^6$ cells (293T) or $10x10^6$ cells (4T1-Luc, E0771, and MDA-MB-231) in 100μL of 10 mM Tris, 150 mM NaCl, 1.5 mM $MgCl_2$, 1% NP-40, pH 9.0. For 4T1-Luc, E0771, and MDA-MB-231, total protein concentration of lysate was measured using the BCA

assay (Pierce, Thermo Fisher), and samples were normalized so the same amount of protein was used for each lysate reaction. The probe $^{32}$P-cGAMP (5 μM) was incubated with mENPP1 (20 nM) or whole cell lysates in 100 mM Tris, 150 mM NaCl, 2 mM $CaCl_2$, 200 μM $ZnCl_2$, pH 7.5 or pH 9.0 for the indicated amount of time. To generate inhibition curves, 5-fold dilutions of ENPP1 inhibitor was included in the reaction. Degradation was evaluated by TLC as previously described[15]. Plates were exposed on a phosphor screen (Molecular Dynamics) and imaged on a Typhoon 9400 and the $^{32}$P signal was quantified using ImageJ. Inhibition curves were fit to obtain $IC_{50}$ values with Graphpad Prism 7.03. $IC_{50}$ values were converted to $K_{i,app}$ values using the Cheng-Prusoff equation $\mathrm{K_{i,app}} = \mathrm{IC_{50}}/(1 + [\mathrm{S}]/\mathrm{K_m})$.

ALPL and ENPP2 inhibition assays

Inhibition assays for other ectonucleotidases were performed by incubating reaction components in 96-well plate format at room temperature and monitoring production of 4-nitrophenolate by measuring absorbance at 400 nM in a platereader (Tecan). ALPL: 0.1 nM ALPL, 2 μM 4-nitrophenyl phosphate, and various concentrations of inhibitor in buffer pH 9.0 containing 50 mM Tris, 20 μM $ZnCl_2$, 1 mM $MgCl_2$ at room temperature. ENPP2: 2 nM ENPP2, 500 μM bis(4-nitrophenyl) phosphate, and various concentrations of inhibitor in buffer pH 9.0 containing 100 mM Tris, 150 mM NaCl, 200 μM $ZnCl_2$, 2 mM $CaCl_2$.

Export assay in cancer cell lines

4T1-Luc, E0771, and MC38 cells were changed to new media supplemented with 50 μM STF-1084. At indicated times, media was collected; cells were scraped off the plate with PBS, pelleted at 1000 rcf, lysed with 4 mL 50:50 acetonitrile:water, and centrifuged at 15,000 rcf. cGAMP was enriched from the media and cell supernatant as described above using the HyperSep Aminopropyl SPE columns and submitted for mass spectrometry quantification.

4T1-Luc tumor mouse model

Seven- to nine-week-old female BALB/c mice (Jackson Laboratories) were inoculated with $5 \times 10^4$ or $5 \times 10^5$ 4T1-Luc-luciferase cells suspended in 50 μL of PBS into the mammary fat pad. When tumor volume (determine length$^2$ x width / 2) reached 80 mm$^3$ to 120 mm$^3$, tumors were irradiated with 20 Gy using a 225 kVp cabinet X-ray irradiator filtered with 0.5 mm Cu (IC-250, Kimtron Inc., CT). Anaesthetized animals were shielded with a 3.2 mm lead shield with a 15 x 20 mm aperture where the tumor was placed. On day 2, 4, and 7 after IR, 100 μL of 100 μM STF-1084 and/or 10 μg cGAMP in PBS or PBS alone were injected intratumorally. Alternatively, 1 mM STF-1084 in PBS or PBS alone were injected intratumorally and 200 μg of anti-CTLA-4 antibody or Syrian hamster IgG antibody (both BioXCell) were injected intraperitoneally on day 2, 5, and 7 after IR. Mice from different treatment groups were co-housed in each cage to eliminate cage effects. The experimenter was blinded throughout the entire study. Tumor volumes were recorded every other day. Tumor volumes were analyzed in a generalized estimation equation in order to account for the within mouse correlation. Pair-wise comparisons of the treatment groups at each time point were done using post hoc tests

with a Tukey adjustment for multiple comparisons. Animal death was plotted in a Kaplan Meier curve using Graphpad Prism 7.03 and statistical significance was assessed using the Log-rank Mantel-Cox test. All mice were maintained at Stanford University in compliance with the Stanford University Institutional Animal Care and Use Committee regulations, and procedures were approved by the Stanford University administrate panel on laboratory animal care.

FACS analysis of tumors

Seven- to nine-week-old female BALB/c WT (4T1-Luc tumors) or C57BL/6 (E0771 tumors) WT, cGAS$^{-/-}$, or STING$^{gt/gt}$ (referred to as STING$^{-/-}$) mice (Jackson Laboratories) were inoculated with 1 x $10^6$ tumor cells suspended in 50 μL of PBS into the mammary fat pad. Two days after injection, tumors were irradiated as described and intratumorally injected with 100 μL of 1 mM STF-1084 in PBS or with PBS alone. For experiments using STING and mENPP1, 100 μL of 100 μM neutralizing STING or non-binding STING (R237A) or 700 nM mENPP1 or PBS were injected intratumorally. On the next day, the tumor was extracted and incubated in RPMI + 10% FBS with 20 μg/mL DNase I type IV (Sigma-Aldrich) and 1 mg/mL Collagenase from Clostridium histolyticum (Sigma-Aldrich) at 37 °C for 30 min. Tumors were passed through a 100 μm cell strainer (Sigma-Aldrich) and red blood cells were lysed using red blood cell lysis buffer (155 mM $NH_4Cl$, 12 mM $NaHCO_3$, 0.1 mM EDTA) for 5 min at room temperature. Cells were stained with Live/Dead fixable near-IR dead cell staining kit (Thermo Fisher Scientific), Fc-blocked for 10 min using TruStain fcX and subsequently antibody-stained with CD11c, CD45, and I-A/I-E (all Biolegend). Cells were analyzed using an SH800S cell

sorter (Sony) or an LSR II (BD Biosciences). Data was analyzed using FlowJo V10 software (Treestar) and Prism 7.04 software (Graphpad) for statistical analysis and statistical significance was assessed using the unpaired t test with Welch's correction.

In vivo imaging

Mice were injected ip with 3mg XenoLight D-Luciferin (Perkin-Elmer) in 200 µl water and imaged using a Lago X in vivo imaging system (Spectral Instruments Imaging). Object height was set to 1.5cm, binning to 4, FStop to 1.2, and the exposure time was 120s. Images were analyzed using aura 2.0.1 software (Spectral Instruments Imaging).

Synthesis of STF-1084

*Preparation of dimethyl (2-(piperidin-4-yl)ethyl)phosphonate*

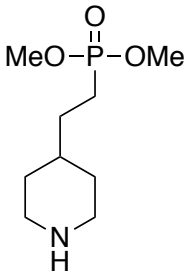


Sodium hydride (2.16 g, 54.11 mmol) was carefully added to a stirred solution of bis(dimethoxyphosphoryl)methane (11.42g, 49.19mmol) in toluene (100 mL) at room temperature. The reaction mixture was then placed under an atmosphere of nitrogen and a solution of 1-benzylpiperidine-4-carbaldehyde (10 g, 49.19 mmol) in toluene (50 mL) was slowly added keeping the temperature below 40 ºC. The resulting mixture was left to stir at room temperature for 16 h and then quenched by the addition of aqueous saturated ammonium chloride solution. The organic phase was separated, washed with

brine, dried ($MgSO_4$) and evaporated to dryness. Chromatography (120 g $SiO_2$; 5 to 100% gradient of EtOAc in hexanes) provided dimethyl (*E*)-(2-(1-benzylpiperidin-4-yl)vinyl)phosphonate (6.2 g, 16%) as a colorless oil.

To a mixture of dimethyl (*E*)-(2-(1-benzylpiperidin-4-yl)vinyl)phosphonate (3.7 g, 12.0 mmol) in ethanol (40 mL) was added Pd/C (1.1 g, 10.3 mmol). The mixture was placed under an atmosphere of hydrogen and stirred at room temperature for 12 h, filtered and evaporated to dryness under reduced pressure to give dimethyl (2-(piperidin-4-yl)ethyl)phosphonate (2.7 g, 100%) as colorless oil.

*Preparation of dimethyl (2-(1-(6,7-dimethoxyquinazolin-4-yl)piperidin-4-yl)ethyl)phosphonate*

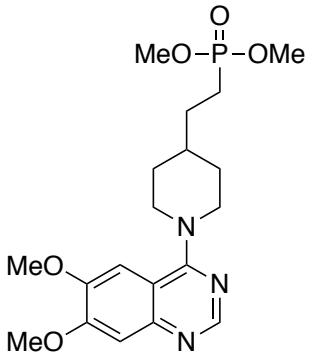


Diisopropylethylamine (0.6 g, 8.9 mmol) was added to a mixture of dimethyl (2-(piperidin-4-yl)ethyl)phosphonate (1.1 g, 4.9 mmol) and 4-chloro-6,7-dimethoxy-quinazoline (1.0 g, 4.5 mmol) in isopropyl alcohol (20 mL). After stirring at 90 ºC for 3 h, the reaction mixture was cooled and evaporated to dryness. Purification of silica gel (5% MeOH in dichloromethane) provided dimethyl (2-(1-(6,7-dimethoxyquinazolin-4-yl)piperidin-4-yl)ethyl)phosphonate (755 mg, 37%) as oil.

LC-MS: m/z = 410.25 $[M+H]^+$

$^1$H NMR (500 MHz, $CDCl_3$) δ 8.65 (s, 1H), 7.23 (s, 1H), 7.09 (s, 1H), 4.19 (dq, *J* = 14.0, 2.9, 2.4 Hz, 2H), 4.02 (s, 3H), 3.99 (s, 3H), 3.77 (s, 3H), 3.75 (s, 3H), 3.05 (td, *J* = 12.8, 2.3 Hz, 2H), 1.93 – 1.77 (m, 4H), 1.67 (ddd, *J* = 14.1, 9.5, 5.9 Hz, 3H), 1.46 (qd, *J* = 12.2, 3.7 Hz, 2H).

*Preparation of dimethyl (2-(1-(6,7-dimethoxyquinazolin-4-yl)piperidin-4-yl)ethyl)phosphonic acid (STF-1084).*

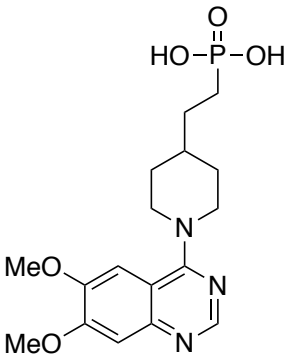


Bromotrimethylsilane (3.67 g, 24 mmol) was added to a cooled solution of dimethyl (2-(1-(6,7-dimethoxyquinazolin-4-yl)piperidin-4-yl)ethyl)phosphonate (3.25 g, 7.94 mmol) in chloroform (60 mL) that was cooled by an ice bath. The reaction mixture was allowed to warm to room temperature and after 90 minutes was quenched by the addition of methanol (20 mL). The mixture was evaporated to dryness under reduced pressure and then solvated in methanol (100 mL). The reaction mixture was concentrated to half volume, filtered to remove precipitate, and then evaporated to dryness. The residue was crystalized with dichloromethane, filtered and dried under vacuum to give dimethyl (2-(1-(6,7-dimethoxyquinazolin-4-yl)piperidin-4-yl)ethyl)phosphonic acid (2.1 g, 69%).

LC-MS: m/z = 381.8 $[M+H]^+$

$^{1}$H NMR (500 MHz, DMSO-$d_6$) δ 8.77 (s, 1H), 7.34 (s, 1H), 7.23 (s, 1H), 4.71 (d, $J$ = 13.1 Hz, 2H), 3.99 (s, 3H), 3.97 (s, 3H), 3.48 (t, $J$ = 12.7 Hz, 2H), 3.18 (s, 1H), 1.97–1.90 (m, 2H), 1.62–1.43 (m, 4H), 1.40–1.27 (m, 2H).

## Extended Data Figures:

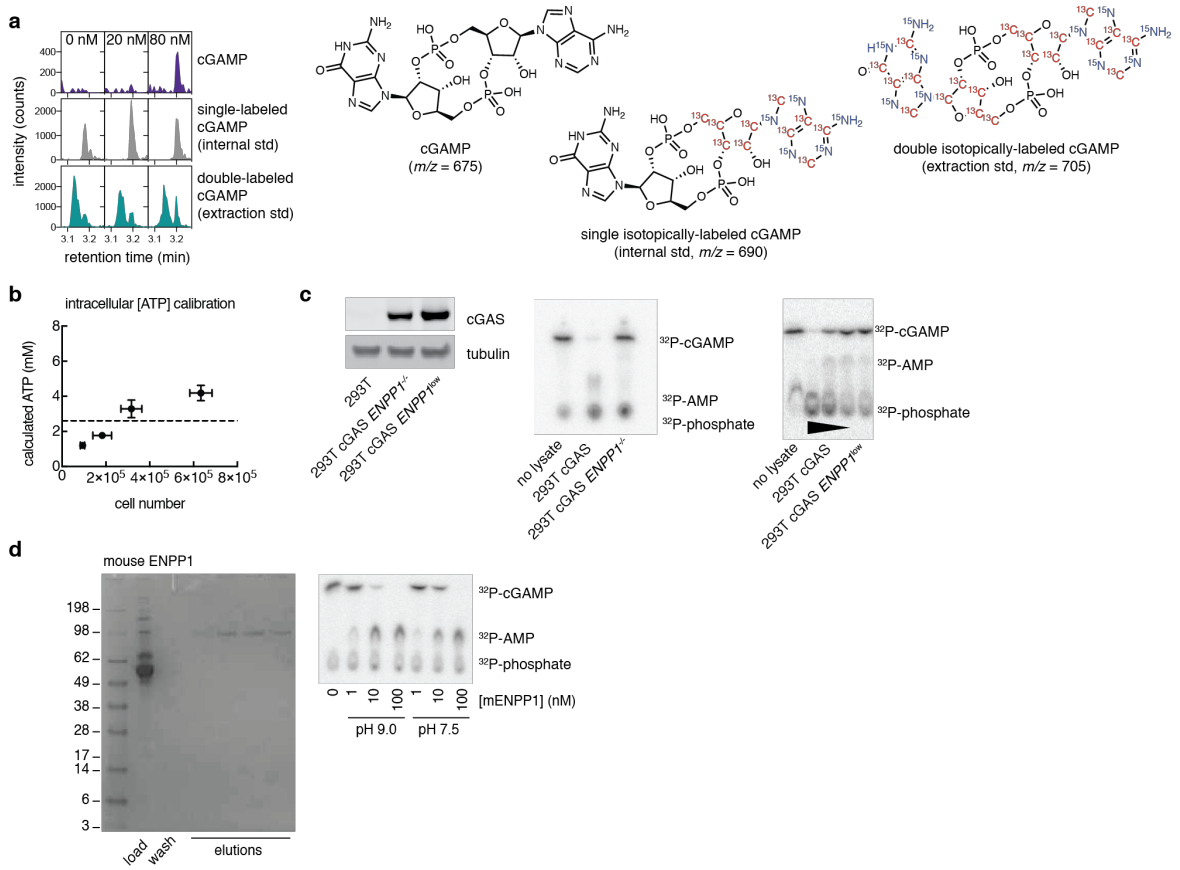


**Extended Data Figure 1 | Developing an LC-MS/MS method and building 293T cGAS ENPP1$^{low}$ and 293T cGAS ENPP1$^{-/-}$ cell lines.**

**a**, Liquid chromatography traces of cGAMP at 0, 20, and 80 nM; single isotopically-labeled internal standard cGAMP (15 Da heavier) at 500 nM; and double isotopically-labeled extraction standard cGAMP (30 Da heavier) at 2 μM. Chemical structures of all analytes.

**b**, Calibration of cell number to ATP concentration measured by LC-MS/MS. Mean ± SEM ($n$ = 2).

**c**, cGAS expression of 293T, 293T cGAS ENPP1$^{-/-}$, and 293T cGAS ENPP1$^{low}$ cell lines analyzed by western blot (left). ENPP1 hydrolysis activity of $^{32}$P-cGAMP in whole cell

lysates from 1 million each of 293T cGAS, 293T cGAS ENPP1$^{-/-}$, and 293T cGAS ENPP1$^{low}$ cells, measured by TLC and autoradiography (right). Lysate data are representative of two independent experiments.

**d**, Coomassie gel of recombinant mouse ENPP1 purified from media; elution fractions were pooled before use (left). $^{32}$P-cGAMP degradation by mouse ENPP1 analyzed by TLC (right).

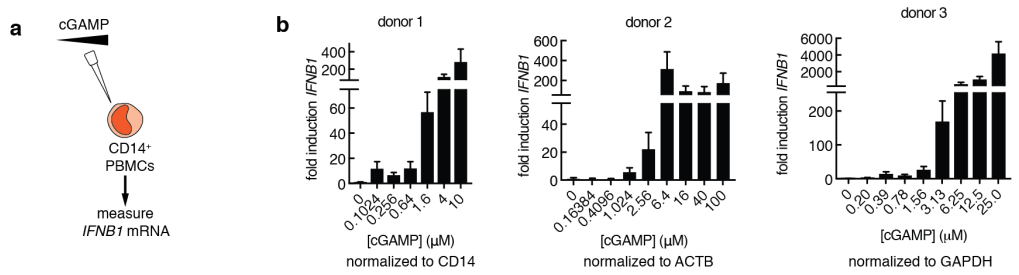


**Extended Data Figure 2 | CD14⁺ PBMCs respond to extracellular cGAMP.**

**a**, Schematic of stimulation of CD14+ PBMCs with extracellular cGAMP. **b**, *IFNB1* induction measured by RT-qPCR for human CD14⁺ PMBCs stimulated with increasing concentrations of extracellular cGAMP for 16 h. Mean ± SEM (*n* = 2 technical qPCR replicates).

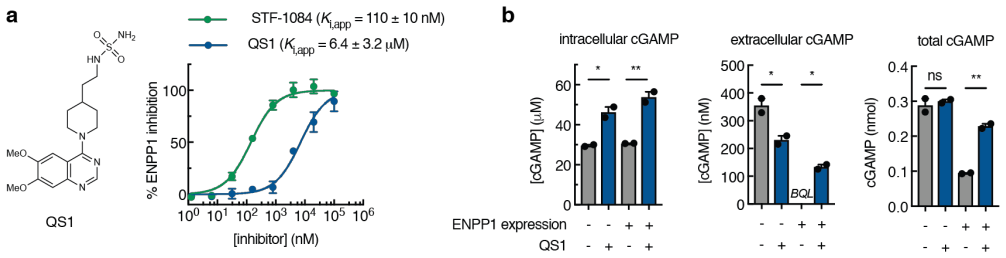


**Extended Data Figure 3 | Improvement of STF-1084 over QS1.**

**a**, Structure of QS1 and its inhibitory activity (compared to STF-1084) against purified mouse ENPP1 with $^{32}$P-cGAMP as the substrate at pH 7.5 (QS1 $K_{i,app}$ = 6.4 ± 3.2 μM). Mean ± SEM ($n$ = 2 independent experiments).

**b**, Intracellular, extracellular, and total cGAMP for 293T cGAS ENPP1$^{-/-}$ cells transfected with empty vector or vector containing human *ENPP1* in the presence or absence of QS1. cGAMP levels were measured after 24 hours by LC-MS/MS. Mean ± SEM ($n$ = 2). *$P$ < 0.05. **$P$ < 0.01 (one-way ANOVA).

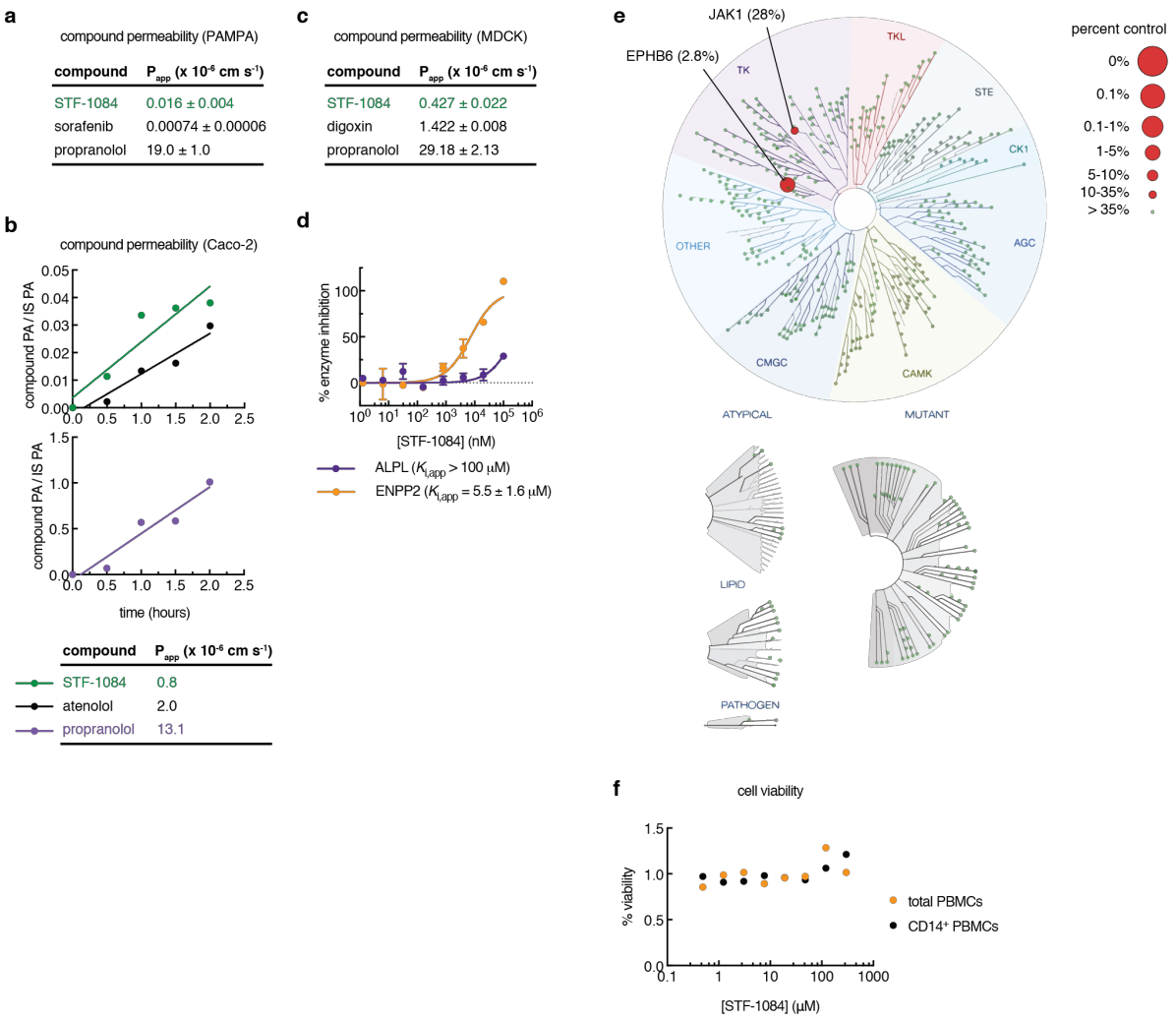


**Extended Data Figure 4 | STF-1084 is cell impermeable, specific to ENPP1, and nontoxic.**

**a**, Permeability of STF-1084 in artificial membrane permeability assay (PAMPA).

**b**, Permeability of STF-1084 in intestinal cells Caco-2 assay. PA = peak area, IS = internal standard. Compounds, including STF-1084, atenolol (low passive permeability negative control) and propranolol (high passive permeability positive control), were incubated on the apical side of a Caco-2 monolayer for 2 hours. Compound concentration on the basolateral side was monitored by LC-MS/MS. Apparent permeability rates ($P_{app}$) were calculated from the slope. Data are representative of two

independent experiments.

**c**, Permeability of STF-1084 in epithelial cells MDCK permeability assay.

**d**, Inhibitory activity of STF-1084 against alkaline phosphatase (ALPL) and ENPP2. Mean ± SEM ($n$ = 2).

**e**, Kinome interaction map (468 kinases tested) for STF-1084 depicting kinase inhibition as a percent of control. Image generated using TREE*spot*™ Software Tool and reprinted with permission from KINOME*scan*®, a division of DiscoveRx Corporation. ©DiscoveRX Corporation 2010.

**f**, Cell viability measured by CellTiterGlo. Total PBMCs and $CD14^+$ PBMCs were incubated with STF-1084 for 16 hours and then assayed for ATP levels using CellTiterGlo. Data was normalized to no STF-1084 to calculate % cell viability.

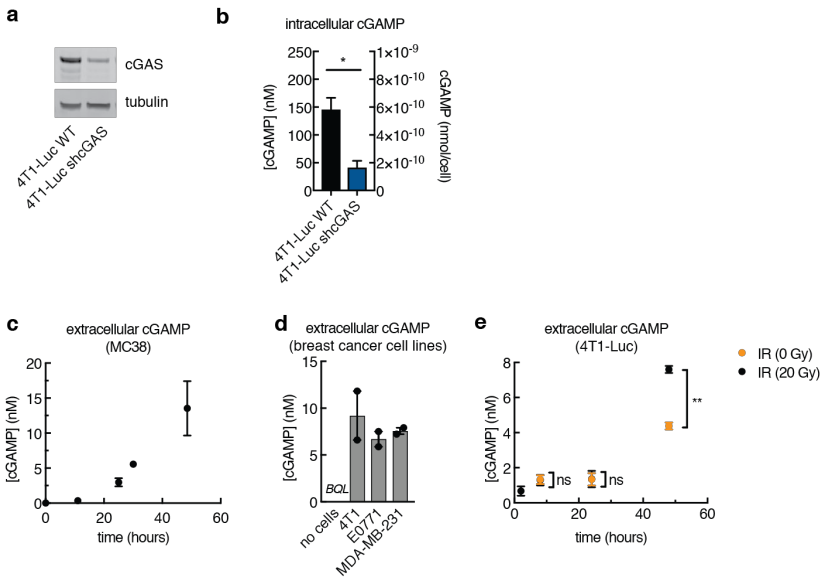


**Extended Data Figure 5 | Cancer cells continuously export cGAMP in culture.**

**a**, cGAS expression of 4T1-Luc WT and 4T1-Luc shcGAS cell lines analyzed by western blot.

**b**, Intracellular cGAMP of 4T1-Luc WT and 4T1-Luc shcGAS cell lines without exogenous stimulation. Mean ± SEM (*n* = 2). 4T1-Luc WT data is repeated from Fig. 4b for comparison.

**c**, Extracellular cGAMP (depicted in media concentration units) of experiment shown in Fig. 4c. Mean ± SEM (*n* = 2).

**d**, Extracellular cGAMP (depicted in media concentration units) of experiment shown in Fig. 4d. *BQL* = below quantification limit. Mean ± SEM (*n* = 2).

**e**, Extracellular cGAMP (depicted in media concentration units) of experiment shown in Fig. 4c. Mean ± SEM (*n* = 2). ***P* = 0.004 (Student's *t* test).

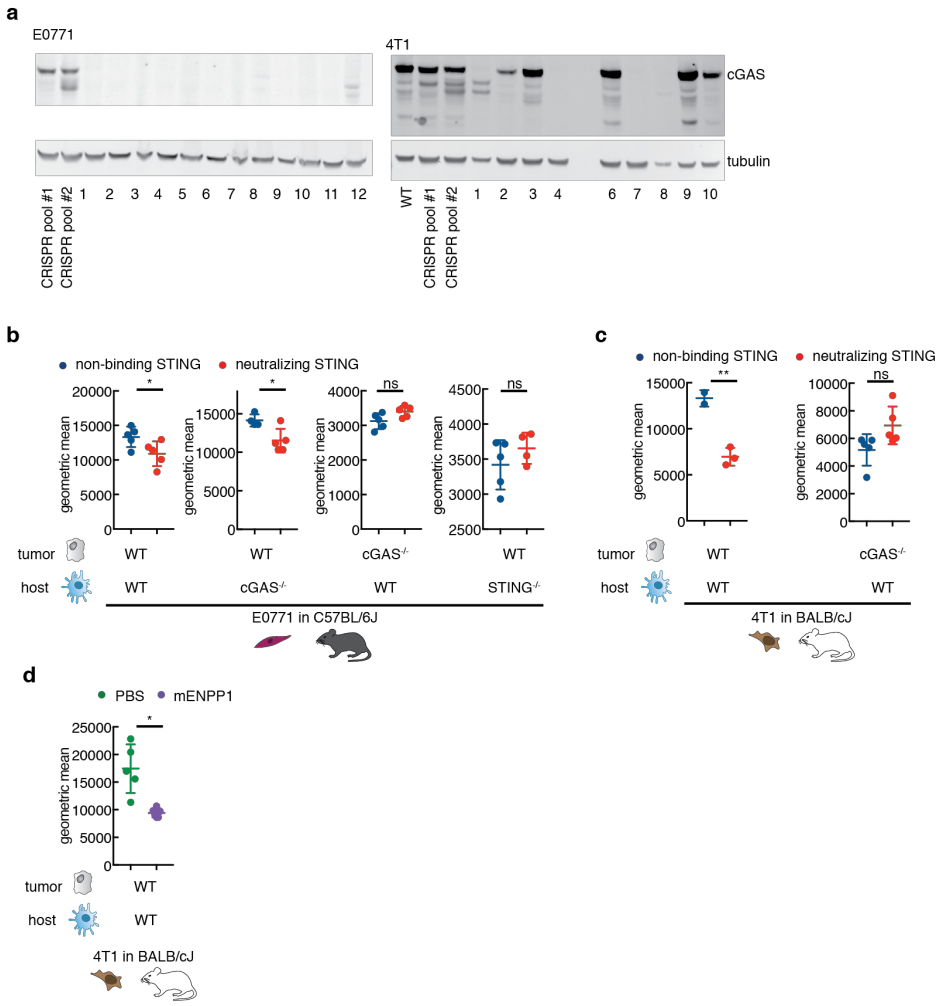


**Extended Data Figure 6 | Sequestration of extracellular cGAMP decreases tumor-associated dendritic cells in a tumor cGAS and host STING dependent manner.**

**a**, E0771 (left) and 4T1-Luc (right) cGAS$^{-/-}$ cells subcloned from CRISPR knockout pools. E0771 cGAS$^{-/-}$ subclones 1, 2, 4, 6, 8, and 9 were pooled before injection into mice. 4T1-Luc cGAS$^{-/-}$ subclones 4, 7, and 8 were pooled before injection into mice.

**b**, Geometric means of experiments shown in Fig. 5g. Mean ± SD. *$P$ = 0.049 (WT tumor/WT host). *$P$ = 0.015 (WT tumor/cGAS$^{-/-}$ host). (Welch's $t$ test).

**c**, Geometric means of experiments shown in Fig. 5h. Mean ± SD. ***P* = 0.009 (Welch's *t* test).

**d**, Geometric means of experiments shown in Fig. 5i. Mean ± SD. **P* < 0.015 (Welch's *t* test).

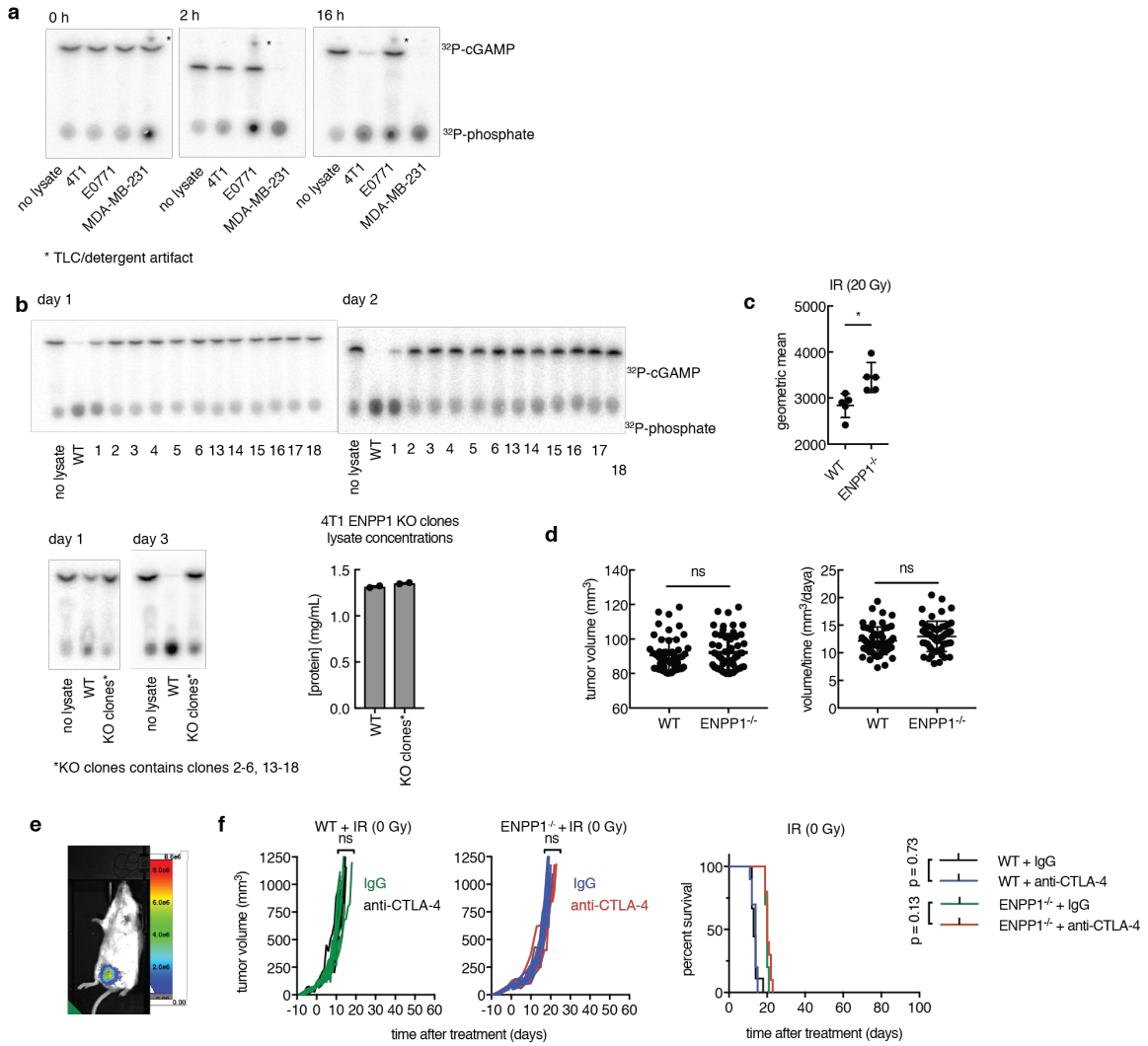


**Extended Data Figure 7 | ENPP1$^{-/-}$ tumors have increased innate immune infiltration, are less aggressive, and are more susceptible to IR and anti-CTLA-4 therapy.**

**a**, ENPP1 activity in 4T1-Luc, E0771, and MDA-MB231 cells using the $^{32}$P-cGAMP degradation assay. Data are representative of three independent experiments.

**b**, Validating ENPP1$^{-/-}$ 4T1-Luc clones using the $^{32}$P-cGAMP degradation assay. Lysates from different clones were normalized by protein concentrations. ENPP1$^{-/-}$ 4T1-Luc clones 2-6 and 13-18 were pooled before injection into mice.

**c**, Geometric means of experiments shown in Fig. 6a. Mean ± SD. *$P$ = 0.012 (Welch's $t$ test).

**d**, (left) Tumor volume of WT ($n$ = 55) vs ENPP1$^{-/-}$ ($n$ = 55) 4T1-Luc cells on the day of treatment; (right) initial tumor growth rate expressed as tumor volume/days needed to reach a size of 100 mm$^3$ ± 20 mm$^3$. Mean ± SD (Welch's $t$ test).

**e**, Bioluminescent image of a tumor-bearing mouse.

**f**, Replotting of data shown in Fig. 6a, b to highlight comparisons between IgG and anti-CTLA-4 treated groups. Established WT or ENPP1$^{-/-}$ 4T1-Luc tumors (100 ± 20 mm$^3$) were treated with three intraperitoneal injections of IgG or anti-CTLA-4 on day 2, 5, and 7 after tumors reached the requisite size. ($n$ = 9 for WT 4T1-Luc + IgG, $n$ = 10 for all other groups). Tumor volumes and Kaplan Meier curves are shown. $P$ values determined by pairwise comparisons using post hoc tests with a Tukey adjustment at day 20 (tumor volumes) and the log-rank Mantel-Cox test (Kaplan Meier).

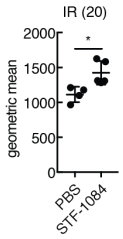


**Extended Data Figure 8 | ENPP1 inhibition synergizes with IR treatment to increase tumor-associated dendritic cells.**

Geometric mean of experiment shown in Fig. 7a. Mean ± SD. *$P < 0.05$ (Welch's *t* test).

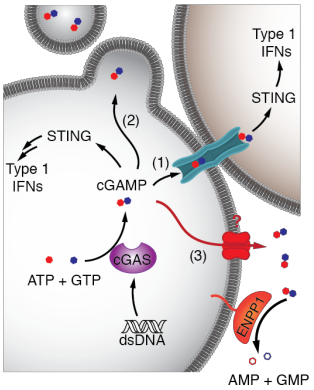


**Extended Data Figure 9 | Different modes of cGAMP transmission from the synthesizing cell to target cells.**

(1) Spread via gap junctions; (2) packaged into budding viral particles and transmitted during the next round of infection; and (3) exported into the extracellular space.

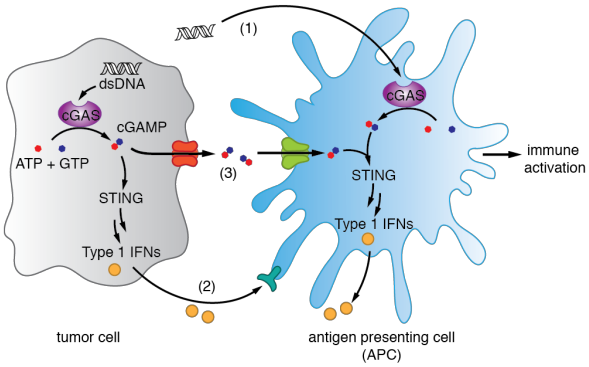


**Extended Data Figure 10 | cGAMP is a cancer danger signal.**

APCs can sense tumor cells through different cGAS-dependent mechanisms: (1) activation of APC cGAS by tumor-derived dsDNA, (2) APC sensing of type I IFNs secreted by tumor cells, and (3) APC sensing of cGAMP constitutively produced and exported by tumor cells.